Supplemental Information for:

Infant and Adult Inhalation Exposure to Resuspended Biological Particulate Matter

Tianren Wu[1,2], Martin Täubel[3], Rauno Holopainen[4], Anna-Kaisa Viitanen[5], Sinikka Vainiotalo[5], Timo Tuomi[5], Jorma Keskinen[6], Anne Hyvärinen[3], Kaarle Hämeri[7], Sampo E. Saari[6], and Brandon E. Boor[1,2*]

[1]Purdue University, Lyles School of Civil Engineering, 550 Stadium Mall Drive, West Lafayette, Indiana 47907, USA

[2]Purdue University, Ray W. Herrick Laboratories, Center for High Performance Buildings, 177 South Russell Street, West Lafayette, Indiana 47907, USA

[3]National Institute for Health and Welfare, P.O. Box 95, Kuopio FI 70701, Finland

[4]Oulu University of Applied Sciences, P.O. Box 222, Oulu FI 90101, Finland

[5]Finnish Institute of Occupational Health, P.O. Box 40, Helsinki FI 00250, Finland

[6]Tampere University of Technology, Department of Physics, P.O. Box 692, Tampere FI 33101, Finland

[7]University of Helsinki, Department of Physics, P.O. Box 64, Helsinki FI 00014, Finland

*Corresponding author,

mailing address: 550 Stadium Mall Drive, West Lafayette, Indiana 47907 USA

e-mail address: bboor@purdue.edu; phone: +1-765-496-0576

Number of Pages: 49

Number of Tables: 6

Number of Figures: 16

Table of Contents

S1. Literature Review

Biological Composition of Indoor Dust & Adverse & Protective Health Effects of Exposure to Microbes & Allergens

Indoor dust in urban homes includes an amazing diversity of bacteria and fungi, but is often dominated by gram-positive bacterial taxa and yeasts associated with the human skin and oral flora, such *Staphylococcus*, *Micrococcus*, *Streptococcus*, *Lactococcus*, *Corynebacterium*, and *Malassezia*, and fungi that are predominantly of outdoor origin (*28, 57, 70, 84*). Mite and animal allergen-carrying particles and pollen grains are also present (*19, 44*). Dust collected from homes on small farms is different in its composition and typically more diverse compared to that in urban and rural residences. It can be heavily enriched with environmental bacteria, including *Acinetobacter sp., Clostridium*, *Lactobacillus spp.*, and *Staphylococcus sciuri*, and animal allergens derived from livestock, fodder, and soil (*18, 80*). While these microbes come from the farm and animal sheds, much of the exposure is occurring indoors, where the *bio*PM is transported via building ventilation and tracked-in on clothing and shoes (*32, 42*).

Exposure to microbes and allergens can cause adverse health effects – a few example studies are referred to in the following. Exposure to bacterial endotoxin (lipopolysaccharides) is associated with increased asthma prevalence and wheezing (*73*). Reponen et al. (*56*) identified specific fungal species as being strongly associated with the development of asthma and Dannemiller et al. (*10*) found increased asthma severity among atopic children to be associated with elevated concentrations of fungi in dust. High concentrations of airborne fungal spores have been positively correlated with frequency of asthmatic attacks and certain fungal spores, such as those of *Aspergillus fumigatus*, and their allergenic proteins can damage epithelia cells and lead to respiratory infections (*14, 50, 43*). Mite allergens, at certain dust concentrations, can lead to the development of mite sensitization, asthma, and allergic rhinitis (*9, 67, 77*). Pollen grains of various plant species, such as ragweed and birch, are coated in allergenic proteins, inhalation of which can cause allergic reactions in a significant fraction asthmatic children and adults (*13, 64, 71*).

Protective health effects ("farm effect," "hygiene hypothesis") associated with exposure to environmental microbes and specific allergens have been identified in numerous studies. Early-life exposures to increased bacterial and fungal diversity and high indoor dust concentrations of bacterial and fungal cells; bacterial lipopolysaccharides and muramic acid; polysaccharides of fungi, pollen, and plants; and allergenic proteins of dust mites and animal dander have been linked to a reduced prevalence of asthma, atopy, wheeze, hay fever, and allergies later in life (*11, 17, 18, 37, 39, 47, 68, 76, 78, 80, 82*). It has been hypothesized that a balanced population of beneficial microbes in the lower and upper airways may provide colonization resistance against pathogenic bacteria and fungi and that exposure to beneficial microbes during infancy may play a key role in shaping the evolution of the respiratory microbiota (*5, 17, 18, 24, 26*).

S2. Supplemental Materials and Methods

Detailed Description of Chamber Setup and Resuspension Experiments

The resuspension experiments were conducted in an 81.4 m^3 environmentally controlled chamber at the Finnish Institute of Occupational Health (FIOH) in Helsinki, Finland from January to March 2015. The walls and floor of the chamber were made of stainless steel and glass. The supply air was filtered with both HEPA and activated carbon filters (Camfil Farr) and the chamber was maintained at a slight positive pressure. Two fans, positioned in opposite corners of the chamber, were used to aid in the mixing of the bulk air (a Philips type HR 3270/B 28W and a Domesto Mod. Gliding Grille, Art.-Nr.: 16401 80). The chamber air exchange rate was 0.66 h^{-1}, as determined by a sulfur hexafluoride (SF_6) tracer gas decay with a multi-gas monitor (Type 1302, Brüel and Kjær). Chamber air temperature and relative humidity (RH) were measured with a HOBO sensor and data logger (HOBO U12-012, Onset Computer Corp., Bourne, MA, USA) and were 23.11±0.77°C and 23.89±4.77% (mean ± s.d.) during the entire measurement campaign.

For the five studied carpets, the residents were asked to refrain from vacuuming their carpets for two weeks. Carpets were carefully folded at the residence, maintaining contact among the upward facing surface, and then carefully transported to FIOH. Each carpet was divided into five paths across its width, with each path being 34 cm wide. Depending on the overall width of the carpet, there was some overlap among the paths. For each path on each carpet, one crawling and one walking resuspension experiment, 45-minutes in duration, were conducted, for a total of fifty individual experiments.

A simplified robotic infant performing a modified belly crawl was used to simulate the crawling locomotion of an infant in a repeatable manner (mass: 4 kg, contact area: 25 cm^2 per hand + 325 cm^2 for lower torso, hand contact frequency: 200 min^{-1}). The robot utilized two high torque servo motors controlled by a microcontroller to simulate the crawling motion of the arms and for forward propulsion. The exterior of the robot was lined with grounded aluminum tape to minimize the accumulation of electrostatic surface charge and was wiped with isopropyl alcohol after each experiment. The walking experiments were conducted by an adult male volunteer wearing a full clean suit outfit with booties and a hood (DuPont™, Tyvek Pro-Tech Suit Classic), nitrile gloves, and a filter mask to minimize particle emissions from the human envelope (mass: 80 kg, height: 188 cm, contact area: 160 cm^2 per foot, footfall contact frequency: 70 min^{-1}). The chamber floor was vacuumed and wiped with isopropyl alcohol after each set of experiments with a given carpet. Measurements were periodically conducted to ensure negligible emissions of FBAPs and total particles from the crawling robot itself and walking in the clean suit outfit, both across the bare, stainless steel flooring of the chamber (N_F and $N_T << 0.1$ cm^{-3}).

Detailed Description of Aerosol Instrumentation

FBAP (N_F) and total (N_T) particle number size distributions (cm^{-3}) were monitored throughout each

resuspension sequence with a LIF-based instrument – the BioScout (1 Hz sampling frequency, nominal sample flow: 2 L min^{-1}) (ENVI BioScout™, Environics Ltd., Mikkeli, Finland) (*59, 60, 61*). The BioScout uses a 200-mW laser diode that emits excitation light at a wavelength of 405 nm (Table S2). After the excitation light impinges on the particle, the scattered light is collected via a photomultiplier tube (PMT) to determine the particle size. The fluorescence emitted by the biological fluorophores in the particle are captured with another PMT and sorted into 16 fluorescence intensity channels. The particles recorded in fluorescence channels 2-16 were classified as FBAPs, with particles in channel 1 considered as non-fluorescent (*59, 60, 61*). The operative size range was optimized between 0.4 and 15.4 μm based on laboratory calibration (16 size fractions). Total (N_T) particle number size distributions were also monitored with an optical particle sizer (nominal sample flow: 1.001 L min^{-1}) (OPS, model 3330, TSI Inc., Shoreview, MN, USA). The measurement size range was 0.314 to 11.2 μm (16 size fractions). As the BioScout data indicated that a significant fraction of the particles was likely of biological origin, a refractive index of 1.4 - 0.003i, representative of general *bio*PM, was used to correct the raw data (*2, 16, 25, 81*). Additional small-chamber experiments with aerosolized dust collected from the five carpets were used to estimate the effective density (ρ_{eff}) of the resuspended particles (1.204 g cm^{-3}) to convert BioScout and OPS particle number concentrations to mass (following Application Note OPS-001 (TSI, 2012), assuming particles to be spherical). All BioScout and OPS data were time-averaged to one minute prior to data analysis. Additionally, an IOM (Institute of Medicine) sampler with 25 mm 0.8 μm pore size MCE (mixed cellulose ester) filters (nominal sample flow: 10 L min^{-1}, cut-off ~100 μm) (SKC Inc., Eighty Four, PA, USA) was used to collect resuspended particles for gravimetric analysis; qPCR analysis for quantification of gram-positive and gram-negative bacteria, selected fungal groups; and bacterial 16S rRNA gene sequencing, as reported in our parallel study, Hyytiäinen et al. (*34*).

A horizontally oriented aluminum tube of length 12 cm was used upstream of the BioScout inlet. The BioScout data was corrected for size-resolved sampling inlet efficiencies and deposition losses in the sample tube (*23, 48*). No sample tubes were used for the OPS. The OPS data was corrected for size-resolved sampling inlet efficiencies (vertically oriented inlet). Settled dust from each carpet was collected at the end of the resuspension experiments using a 37 mm MCE filter cassette and nylon sock for gravimetric, optical particle counting (via PAMAS SVSS, PAMAS GmbH, Rutesheim, Germany), and microbial analysis.

Analysis of FBAP Size Distributions, Respiratory Tract Deposited Dose Rates, and Emission Rates

All BioScout and OPS data were processed and analyzed with custom-written scripts in MATLAB (The MathWorks, Inc., Natick, MA, USA). For each resuspension experiment (crawling or walking path), the mean FBAP (N_F) and total (N_T) particle number size distributions were fitted with a unimodal lognormal distribution (Equation S1) (*65*). The geometric mean diameter ($\overline{D_{pg,i}}$), geometric standard deviation ($\sigma_{g,i}$), and particle number concentration or amplitude (A) in each mode were determined by the least squares

method. *Note: here we use log_e in our lognormal fitting function.*

$$\frac{dN}{dlogD_p} = \frac{A}{(2\pi)^{1/2}\log_e(\sigma_g)} \exp\left[-\frac{(\log_e D_p - \log_e \overline{D_{pg}})^2}{2\log_e{}^2(\sigma_g)}\right] \quad \text{(S1)}$$

To evaluate the amount of resuspended FBAPs (*bio*PM proxy) that deposit in the infant and adult respiratory system, the total and regional FBAP number and surface area respiratory tract deposited doses (# or μm^2 of deposited FBAPs) were estimated using Equations S2 and S3. We assume that during the crawling or walking periods, the infant and adult are exposed to a constant FBAP concentration, which is defined by the carpet-averaged mean N_F size distributions measured on each carpet in the BZ during the resuspension periods ($dN_F/dlogD_p$ (cm^{-3})). In Equations S2 and S3, the subscripts *i* and *j* denote the particle size fraction (D_{p1} to D_{p2}) and the region of respiratory tract (head airways, tracheobronchial region, and pulmonary region), respectively. The doses are then expressed as FBAP respiratory tract deposited dose rates (*RTDDR*$_F$*s*) (# or μm^2 of FBAPs deposited per minute) by normalizing by an exposure period (t_1 to t_2) of one minute of crawling or walking. To convert from number to surface area concentration, the geometric midpoint diameter of each size fraction was used and the FBAPs were assumed to be spherical.

$$Number\ Respiratory\ Tract\ Deposited\ Dose_{i,j} = \int_{t1}^{t2}\int_{D_{p1}}^{D_{p2}} \frac{dN_F}{dlogD_p} \times \dot{V}_E \times DF_{i,j} \times dlogD_p \times dt \quad \text{(S2)}$$

$$Surface\ Area\ Respiratory\ Tract\ Deposited\ Dose_{i,j} = \int_{t1}^{t2}\int_{D_{p1}}^{D_{p2}} \frac{dN_F}{dlogD_p} \times \dot{V}_E \times DF_{i,j} \times \pi D_p^2 \times dlogD_p \times dt \quad \text{(S3)}$$

Size-resolved deposition fractions ($DF_{i,j}$) as a function of particle aerodynamic diameter for the infant and adult respiratory tract were obtained from the open-source Multiple-Path Particle Dosimetry (MPPD) Model (v3.04, Applied Research Associates, Inc., Albuquerque, NM, USA) (Figure S6). The MPPD model accounts for the inhalable fraction of particles for a given breathing route. The MPPD model conditions that were selected to best represent the exposure scenario are as follows: the age of the infant and the adult are 3 months and 21 years, respectively; the upper body of the infant is leaning forward while crawling, while the body of the adult is upright; nasal breathing route for the adult; and nasal and oral breathing routes for the infant. The respiratory minute volume ($\dot{V}_E = f \times V_T$), breathing frequency (*f*), and tidal volume (V_T) for an infant under 1 year of age in light activity were assumed to be (from Hofmann et al. (*27*)): 0.00598 $m^3\ min^{-1}$, 32 min^{-1}, and 187 mL, respectively, and for an adult in light activity (*79*, average of male and female): 0.0195 $m^3\ min^{-1}$, 18 min^{-1}, and 1083 mL, respectively. Weight-normalized *RTDDR*$_F$*s* ($min^{-1}\ kg^{-1}$) were also calculated, assuming infant and adult body masses of 9.2 kg (6-12 months) and 80 kg, respectively (*79*).

Hygroscopic growth of inhaled *bio*PM in the respiratory tract, where the air approaches saturation (RH ~ 99.5%), is likely (*33, 38, 41, 54, 55*). The impact of hygroscopic growth was evaluated by comparing

RTDDR$_F$*s* for two cases: (1.) no particle growth and (2.) correcting the inhaled BZ FBAP size distributions with a hygroscopic growth factor (GF) of 1.12, which represents the median of maximum GFs reported for various bacterial and fungal species at 98% RH (*15*).

Size-resolved FBAP emission rates (E_i^W, # of FBAPs emitted per hour) for the adult walking-induced resuspension experiments, where the chamber air was reasonably well-mixed given the intensity of human movement and use of two mixing fans, were determined through application of a single-zone material balance model*:*

$$V\frac{dC_i}{dt} = AER \cdot V \cdot C_{Out,i} - AER \cdot V \cdot C_i - \beta_i \cdot V \cdot C_i + E_i \quad \text{(S4)}$$

where, V is the volume of the chamber (cm^3); C_i is the FBAP number concentration in the chamber for a given particle size fraction *i*, measured at the adult BZ height (cm^{-3}); AER is the air exchange rate of the chamber (h^{-1}); $C_{Out,i}$ is the FBAP number concentration in the chamber supply air (cm^{-3}); β_i is the first-order deposition loss rate coefficient (h^{-1}); and E_i is the FBAP emission rate during adult walking (# of FBAPs emitted per hour). E_i^W was then estimated using Equation S5 for a given particle size fraction *i* (from Zhou et al. (*87*)):

$$E_i^W = V \times \left[\frac{\Delta C_i^W}{t_W} + (\beta_i + AER) \times \overline{C_i^W}\right] - V \times \left[\frac{\Delta C_i^B}{t_B} + (\beta_i + AER) \times \overline{C_i^B}\right] \quad \text{(S5)}$$

ΔC_i^W and ΔC_i^B (cm^{-3}) represent the difference in FBAP concentration between the beginning and end of a 20-minute walking resuspension period (W, t_W) and the 10-minute background period (B, t_B) in the walking tests, respectively. $\overline{C_i^W}$ and $\overline{C_i^B}$ (cm^{-3}) represent the mean FBAP concentration measured during the resuspension period and background periods in the walking tests, respectively. Size-resolved first-order deposition loss rate coefficients (β_i) were estimated from the 15 minute decay period (Figure S5) and are in agreement with previously published empirical estimates (*3*, *4*, *72*, *85*).

It should be noted that the emission rate analysis presented in this study is influenced by mixing conditions of the bulk chamber air as the adult volunteer walked across the carpet, which were deliberately enhanced through use of two mixing fans positioned in opposing corners of the chamber, as well as variations in relative humidity among the experiments (23.89±4.77%), the latter of which can affect the adhesion forces (e.g. capillary and electrostatic forces) acting on the settled *bio*PM (e.g. Qian et al. (*54*)).

Statistical Analysis

The Mann-Whitney test was used to evaluate the impact of activity patterns (crawling and walking) and differences in carpets on the exposure to resuspended FBAPs and *RTDDR*$_F$, as well as the impact of

breathing routes on the infant $RTDDR_F$s. *p*-values below 0.05 were considered statistically significant. To compare the carpet-averaged resuspended N_F and N_T with the total bacterial and fungal concentrations (via qPCR) in the air and carpet dust, dust load, and total particle number concentration (>1 μm) in carpet dust (via PAMAS), *p*-values (Wilcoxon signed rank test) and Pearson correlation coefficients were calculated in MATLAB. The total particle number concentration (>1 μm) in carpet dust was also compared with the total bacterial and fungal concentration in carpet dust. Results are presented in Tables S5 and S6.

S3. Supplemental Results and Discussion

Comparison between BioScout and OPS Total Particle Number Size Distributions

The magnitude and shape of the mean total particle size distributions ($dN_T/dlogD_p$ (cm^{-3})) measured by both the BioScout and OPS agreed very well during the walking experiments (adult BZ sampling) for each of the five carpets, as shown in Figure S9. In contrast, distinct differences in the magnitude of the total particle size distributions were observed in the crawling experiments (Figure S9). We hypothesize that this is due to spatial variability in concentrations of resuspended particles within and around the infant personal cloud. Due to the layout of the mobile trolley, the sampling inlets of the two instruments were not identical within a plane at infant BZ height (see Figure S3), with the OPS inlet recessed 10 cm further back from the edge of the crawling path compared to the BioScout inlet. The total particle size distributions for the BioScout were roughly a factor of two greater than those reported by the OPS, for all particle sizes > 0.8 μm. This may suggest that the resuspended particle cloud around the robot was highly spatially variant at a length scale on the order of 10 cm, with particle concentrations decreasing radially outward from the crawling path. In the above, we assume nearly identical counting statistics for both instruments (> 1 μm) and have corrected the raw data for sampling inlet efficiencies and deposition losses in the BioScout sample tube.

Size-Resolved Emission Rates of Resuspended bioPM (FBAPs) During Walking

Figure S14 presents the size-resolved lognormalized emission rates of resuspended FBAPs during the adult walking experiments on each of the five carpets ($dE_F/dlogD_p$, # of FBAPs emitted per hour). For comparison, per-person FBAP emission rates from Bhangar et al. (*3*) (transition periods in a classroom) and Bhangar et al. (*4*) (walking on carpeted flooring in a chamber) are also shown, assuming a CO_2 emission rate during walking of 38 g/min (*4*). The lognormalized FBAP emission rate distributions exhibited a primary mode between 2 and 5 μm, with a shoulder from 6 to 9 μm and a second, weaker mode developing for particles > 9 μm. The dominant peak between 2 and 5 μm is consistent with the FBAP emission rates reported by Bhangar et al. (*3*, *4*). qPCR-based emission rates follow a similar trend, with Qian et al. (*52*) reporting a predominant peak between 3 and 5 μm (aerodynamic diameter) for bacteria in an occupied classroom and Hospodsky et al. (*30*) reporting dominant peaks in bacterial and

fungal emission rates in the range of 4.7 and 9 μm (aerodynamic diameter).

Figure S14 summarizes size-integrated (1-10 μm) mean FBAP emission rates during walking on each of the five carpets, along with FBAP emission rates reported by Bhangar et al. (*4*) and Zhou et al. (*87*) (FBAP emissions from three volunteers with and without applying skin moisturizer) and total particle emission rates for walking induced resuspension (*20, 51, 53, 74*). Walking on carpet was found to release on the order of 10^8 to 10^9 FBAPs per hour. Thus, in only one minute of walking, one would resuspend 1 to 10 million FBAPs. Carpet dust offers a plentiful supply of *bio*PM, with total bacterial and fungal loads ranging from 10^8 to 10^9 CE/m^2 (Table S1). There was nearly an order of magnitude difference in total FBAP emissions between carpets 4 (cotton) and 5 (wool), despite containing a similar number of settled bacterial and fungal cell equivalents, 5.15 x 10^8 and 4.37 x 10^8 CE/m^2, respectively. This demonstrates that the structure of the dust deposit along the depth of the carpet fibers, interaction between the fibers and human foot during contact, and impact of carpet fiber material on particle adhesion forces likely all play a role in affecting the number of FBAPs that resuspend.

The FBAP emission rates reported in this study are greater than those reported by Bhangar et al. (*3, 4*) and Zhou et al. (*87*), but lower than those reported for total particles for walking-induced resuspension as summarized in Qian et al. (*53*) (based on data from Ferro et al. (*20*), Qian et al. (*51*), Tian et al. (*75*)). This may be due in part to the magnitude of available *bio*PM in the carpet dust for resuspension. In this study, the carpets were not cleaned for at least two weeks prior to the measurements, with dust loads in the range of 2.6 to 5.3 g/m^2 (carpets 1, 3, 4, 5) and 16.7 g/m^2 (carpet 2). In Bhangar et al. (*3*), custodial cleaning was conducted daily in the classroom, and in Bhangar et al. (*4*) the carpeted floor was vacuumed daily. Qian et al. (*51*) evaluated resuspension for a dust load of 20 g/m^2 and Tian et al. (*74*) studied 2 and 8 g/m^2. The lower FBAP emission rates reported in the present study, as compared to the total particle emission rates summarized in Qian et al. (*53*), may be due in part to the low N_F/N_T ratios for sub-2 μm particles, which do resuspend in meaningful quantities (Figures 2, S8). As the net number of particles that resuspend from a surface (not necessarily the resuspension fraction) generally increases with dust loading (*7, 8*), this may explain the difference in FBAP emission rates, but other factors, such as the footfall contact frequency, carpet fiber material, chamber relative humidity, and chamber bulk air mixing conditions will likely affect the emission rates reported in Figure S14. The FBAP emission rates in this study are one to two orders of magnitude greater than those reported for particle release from the human envelope by Zhou et al. (*87*). Thus, walking-induced resuspension may play a more dominant role in elevating indoor concentrations of *bio*PM compared to direct skin shedding, which is consistent with the results reported in Hospodsky et. al. (*28*) and Adams et al. (*1*).

Infant Crawling-Induced and Adult Walking-Induced Resuspension Mechanisms

Both the belly crawling of an infant and walking (footfalls) of an adult contribute to appreciable

resuspension of *bio*PM from carpet dust. While the latter is well characterized for abiotic particles (*53*), the former has received little attention, with only several studies attempting to investigate near-floor exposures of infants and children (*62*, *66*, *83*). In this study, it is likely that differences in body mass, contact area, and contact frequency between the adult volunteer (mass: 80 kg, height: 188 cm, contact area: 160 cm^2 per foot, footfall contact frequency: 70 min^{-1}) and the simplified robotic infant (mass: 4 kg, contact area: 25 cm^2 per hand + 325 cm^2 for lower torso, hand contact frequency: 200 min^{-1}) influenced the resuspension process and resulting number of resuspended FBAPs. The differences in the nature of contact and applied surface pressure likely induce different airflow patterns and surface vibrations at and near the point of contact of the body with the carpet, which were not characterized in this study. Gomes et al. (*22*) demonstrated that the dominant mechanism of walking-induced resuspension is the highly impulsive airflow generated at and near the point of contact between the foot and the floor. It is unknown if this holds true for crawling. Contact electrification likely plays a significant role in affecting the magnitude and directionality of the electrostatic adhesion forces acting on the *bio*PM for crawling-induced resuspension, given the repetitive nature of contact and separation between the body and carpet fibers, along with the large surface area in contact with, and sliding against, the carpet fibers (e.g. lower torso for belly crawling) (*35*, *36*, *86*).

LIF-Based Exposure Assessment: Comparisons with Indoor Dust and qPCR Analysis

It is important to draw comparisons between LIF and two other important and commonly employed parameters in indoor microbial exposure assessments: dust loading in the carpets and DNA-based analysis from carpets and BZ air. The carpet dust mass loading (g/m^2) was found to be a poor predictor of the number of resuspended FBAPs an infant or adult will be exposed to (correlation coefficients (r's) and *p*-values for crawling: -0.308 and 0.019 and walking: 0.179 and 0.014), while a marginal trend was observed between FBAP concentrations and the number of settled particles ($\#/m^2$, r's and *p*-values for crawling: 0.344 and 0.134 and walking: 0.828 and 0.134) or bacterial and fungal CEs (CE/m^2, r's and *p*-values for crawling: -0.160 and 0.065 and walking: 0.093 and 0.065) in the carpet dust (Figure S7a,b,c and Tables S1, S6). While crawling on carpets 2 and 3 contributed similar levels of FBAPs to the infant BZ, 0.858 and 0.882 cm^{-3}, respectively, carpet 2 had a dust load 3.17-fold greater than carpet 3 with 3.44 times as many bacterial and fungal CEs. Carpet 1 was associated with the highest FBAP concentration in the infant BZ (2.257 cm^{-3}), but had the fourth lowest loadings of particle mass (2.79 g/m^2) and number (2.28 x 10^9 $\#/m^2$) among the four carpets. These results demonstrate that relying solely on settled floor dust analysis will result in exposure mischaracterizations for resuspended *bio*PM.

In comparing LIF and qPCR, several factors must first be discussed. LIF typically serves as a lower limit for total *bio*PM and is subject to non-microbial fluorescent interferents, for which limited data exists for sampling in indoor environments. The accuracy of qPCR in reporting true concentrations of airborne bacteria and fungi is limited by poor extraction efficiencies for DNA from cells and cells from filter

substrates, along with possible DNA degradation during sampling and storage (*21*, *29*). Hospodsky et al. (*29*) reported overall extraction efficiencies (η) for selected bacterial cells and fungal spores on different filter media to range from about 3% to over 10%. If species- and filter-specific extraction efficiencies are unknown and not accounted for, true microbial concentrations can be underpredicted by well over one order of magnitude, thus making quantitative comparisons with LIF difficult. As that is the case in this study, FBAP concentrations were compared against total bacterial and fungal CE concentrations for a range of possible overall extraction efficiencies: 1, 5, 10, and 20%. As shown in Figure S7e, the overall extraction efficiency is likely between 1 and 5%, within the range reported by Hospodsky et al. (*29*), however, this analysis may be biased by weakly fluorescent *bio*PM and non-microbial fluorescent interferents and – to some extent possibly – quantification of free DNA as cells and an unknown contribution of *bio*PM collected up to ~100 μm with the IOM sampler (BioScout only captured *bio*PM up to 15.4 μm). While these issues can hinder absolute quantitative comparisons between LIF and qPCR, they would less impact on the relative comparisons between LIF and qPCR shown in Figure S7 (r's and *p*-values for BZ crawling: -0.550 and 0.021 and walking: 0.021 and 0.014). The total particle number concentration in the carpet dust (> 1 μm) was also compared against qPCR (Figure S7d). For three of the five carpets, the number of total particles were approximately twice that of total bacterial and fungal CEs. Given that the qPCR values are likely underestimates of the true concentrations, this demonstrates that a significant fraction of coarse-mode settled particles are of biological origin.

The results of LIF-based exposure assessments will be affected by the particular type of LIF-based aerosol instrument employed, e.g. BioScout, Wideband Integrated Bioaerosol Sensor (WIBS), and Ultraviolet Aerodynamic Particle Sizer (UV-APS) (*31*). Different types of LIF-based aerosol instruments adopt excitation and detection bands at different wavelengths (Table S2). In addition, the strategies to determine the fluorescence threshold, beyond which a particle can be classified as an FBAP, can be very different and significantly affect the results. Thus, comparisons of FBAP measurements between different LIF techniques can be challenging. In addition, LIF techniques lack of the ability to accurately discriminate the types of *bio*PM (e.g. bacterial cells, fungal spores, pollen grains). Even though advanced data analysis methods based on hierarchical agglomerative cluster analysis were developed for the WIBS to classify the *bio*PM (e.g. Robinson et al. (*58*)), the uncertainty of classification should always be considered due to the unknown fraction of contaminating particles in each cluster, and it is difficult to apply to the instruments with a single excitation source and fluorescence detector, such as the BioScout and UV-APS.

Study Limitations

An important limitation of this study is the crawling motion of the simplified robotic infant, which only represents a single crawling style at a given contact frequency (modified belly crawl) and cannot capture the true complexity of the locomotion of an infant. It is likely that resuspension would vary with a

particular crawling style, such as hands-and-feet crawling compared to creeping (*45*), and with age, as the infant learns to walk. Advanced anatomically-correct robotic platforms could be developed to simulate these movements, and their associated contact frequencies, more accurately and evaluate their impact on the resuspension of *bio*PM. Differences in room airflow distribution and mixing conditions between this chamber study and real-world conditions will affect the measured *bio*PM concentrations in the BZ. In addition, the tested carpets were collected from residences in Finland, where it is not common to wear shoes indoors. It is likely the dust loading and microbial composition would be different for homes in other countries where shoes are worn indoors (e.g. track-in effect). The $RTDDR_F$ analysis can be improved by accounting for the non-sphericity of *bio*PM through size-resolved dynamic shape factors specific to different *bio*PM types, measurement of FBAP aerodynamic diameter-based size distributions, and application of actual GFs (*55, 69*). Lastly, the utility of LIF for $RTDDR_F$ analysis of resuspended *bio*PM can be further assessed through comparison with size-resolved qPCR analysis of bacteria and fungi and application of known DNA and filter extraction efficiencies for the given sampling and analysis protocol.

Tables

Table S1. Summary of tested carpets and dust deposits.

Carpet ID	Residence & Location	Location of Carpet in Residence	Carpet *l* x *w* (m)	Carpet Material	Carpet Type	No. Occup.	No. Pets	Dust Load (g/m^2)*	Total Surface Number Concen. > 1 μm ($\#/m^2$)**	Gram + Bacterial Concen. in Dust (CE/m^2)***	Gram - Bacterial Concen. in Dust (CE/m^2)***	Total Fungal Concen. in Dust (CE/m^2)***	Total Bacterial & Fungal Concen. in Dust (CE/m^2)***
1	R1, Helsinki	Bedroom	2.32x 1.73	Wool	Finnish Woven	2	1, cat	2.79	2.28×10^9	1.01×10^9	1.85×10^8	8.55×10^6	1.20×10^9
2	R2, Helsinki	Living Room	2 x 1.4	50% Wool, 50% Sisal	Jute	4	0	16.72	7.30×10^9	1.91×10^9	1.16×10^9	3.87×10^7	3.11×10^9
3	R1, Helsinki	Corridor	1.95 x 1.33	Worsted Wool	Knotted, Pile-Woven	2	1, cat	5.26	5.34×10^9	7.00×10^8	1.99×10^8	3.88×10^6	9.03×10^8
4	R3, Helsinki	Living Room	1.44 x 1.3	Cotton	Jute	2	0	2.63	1.06×10^9	3.40×10^8	1.49×10^8	2.54×10^7	5.15×10^8
5	R4, Helsinki	Living Room	2.33 x 1.6	Wool	Knotted, Pile-Woven	1	0	4.52	2.53×10^{10}	2.17×10^8	2.00×10^8	1.94×10^7	4.37×10^8

*: Sieved dust load from filter cassette samples loads (pore size 1 mm x 1 mm).
**: Determined via optical particle counting with a PAMAS SVSS.
***: via qPCR analysis of carpet dust, presented in Hyytiäinen et al. (*34*)

Table S2. Comparison of operational parameters of three LIF-based aerosol instruments.

LIF-Based Aerosol Instrument	Particle Size Range	Excitation Wavelength (λ_{ex}, nm)	Emission Wavelength (λ_{em}, nm)
BioScout, Environics Ltd. (*59*) (used in present study)	0.4-15.4 μm	405	> 442
WIBS-NEO, DMT Inc. (*88*)	0.5-50 μm	280, 370	310-400, 420-650
UV-APS, TSI Inc. (*59*)	0.5-20 μm	355	430-580

Table S3. List of possible non-microbial fluorescent interferents in the present study.

Non-Microbial Fluorescent Interferents	Possible Origin in Carpet Dust of the Present Study	λ_{ex} (nm)	λ_{em} (nm)	Relevance to the Present Study
Polycyclic aromatic hydrocarbon-(PAH)-containing particles (*49*)	Combustion-generated aerosols, both indoors and outdoors of residence in which carpet was located.	230-390 (*49*)	310-540 (*49*)	While fluorescent, interference is primarily of concern for particles in the sub-micron range. We observed minimal concentrations of resuspended FBAPs < 1 μm, thus, this was not a relevant interferent.
Soot (*49, 63*)	Combustion-generated aerosols from engines and biomass burning, can be transported from outdoors to indoors.	Unknown	Unknown	Previously detected by the WIBS as FBAPs (*63*), they are possibly present in the dust, but are unlikely to contribute significantly to coarse-mode resuspended FBAPs.
Secondary organic aerosol (SOA) (*49*)	Oxidation of volatile organic compounds (VOCs), both indoors and outdoors of residence in which carpet was located.	280-425 (*49*)	360-490 (*49*)	While fluorescent, interference is primarily of concern for particles in the sub-micron range. We observed minimal concentrations of resuspended FBAPs < 1 μm, thus, this was not a relevant interferent.
Humic-like substances (HULIS) associated with soil particles (*49, 63*)	Tracked-in from outdoors on shoes and transferred to carpet via contact transfer.	230-500 (*49*)	350-600 (*49*)	Most HULIS and mineral dust exhibit low fluorescence intensity and may not cause significant interference with fluorescent *bio*PM (*49*), while certain types of mineral dusts and HULIS present high fluorescence intensity (*63*). They are likely present in indoor dust to varying extents and may contribute to the resuspended FBAPs reported in the present study. It is also possible that resuspended soil and mineral particles may act as carriers for *bio*PM, making them fluorescent.
Mineral dust (*49, 63*)				

Squames (skin cells and cell fragments) (*6*)	Desquamation by humans and pets living in residence in which carpet was located.	Range, depending on protein, co-enzyme, or skin pigment (*6*)	Range, depending on protein, co-enzyme, or skin pigment (*6*)	Squames are the most likely non-microbial interferent that may bias the resuspended FBAP data reported in the present study. Skin cells can contain fluorescing proteins, co-enzymes, and skin pigments (*6*). However, as >90% of skin fragments are larger than 10 μm in size (*40*), the interference will predominately affect concentrations of the super-10 μm FBAPs. Squames can also serve as carriers of skin-associated bacteria (*12*) and may agglomerate with *bio*PM in dust deposits, making them fluorescent.
Particles from clothing fabrics (*63*) Coloring and fluorescent whitening agents in fabric fibers and detergent residue (*3, 46, 75, 89, 90*)	Clothing and carpet fibers that have accumulated in dust deposit.	Unknown	Unknown	Particles from clothing fabric have been detected by the WIBS as FBAPs in previous measurements (*63*). These particles and carpet/fabric fibers containing fluorescent whitening agents may exist in indoor dust and resuspend. However, given the high fraction of bacterial and fungal cells detected in our carpet dust samples (Table S1, Figure S7), it is likely they did not significantly bias the FBAP data.
Dust mite and animal allergen-carrying particles	Mites in carpet dust and animal dander.	Unknown	Unknown	Both can be associated with sub-10 μm particles (*44*) and may have been detected as FBAPs, but their fluorescent properties are presently unknown.

Table S4. Summary tables for the fifty crawling and walking resuspension experiments.

Carpet	Movement	Test	Path	Temperature (°C) (mean ± standard deviation)	Relative Humidity (%) (mean ± standard deviation)	BioScout											
						N_F (cm^{-3})	$N_{F,bgd}$ (cm^{-3})	N_T (cm^{-3})	$N_{T,bgd}$ (cm^{-3})	$dN_F/dlogDp$ $Mode_{FBAP}$			$dN_T/dlogDp$ $Mode_{Total}$			M_F (μg m^{-3})	M_T (μg m^{-3})
										A (cm^{-3})	D_{pg} (μm)	σ_g	A (cm^{-3})	D_{pg} (μm)	σ_g		
1	Crawling	n = 1	A	23.34 ± 0.11	25.98 ± 0.93	2.513	0.017	5.014	0.082	2.33	3.64	1.62	4.05	2.64	1.97	527.70	538.24
		n = 2	B	23.66 ± 0.08	27.18 ± 0.86	2.119	0.044	4.484	0.128	1.92	3.71	1.52	3.24	2.87	1.81	388.08	399.48
		n = 3	C	23.85 ± 0.07	27.31 ± 0.52	2.666	0.116	4.685	0.685	2.53	3.69	1.59	4.33	2.73	1.89	484.90	500.80
		n = 4	D	23.94 ± 0.05	27.46 ± 0.71	2.440	0.095	4.704	0.233	2.24	3.85	1.67	3.64	2.91	1.96	686.45	701.92
		n = 5	E	24.07 ± 0.07	26.63 ± 0.91	1.539	0.057	3.170	0.123	1.50	3.78	1.61	2.54	2.80	1.92	392.59	400.33
		Mean		23.76 ± 0.26	26.90 ± 1.52	2.255	0.066	4.411	0.250	2.11	3.73	1.61	3.76	2.69	1.99	495.94	508.16
2	Crawling	n = 6	A	23.97 ± 0.09	25.59 ± 0.57	0.958	0.048	1.466	0.181	0.75	4.06	1.68	1.06	3.42	1.95	472.00	476.50
		n = 7	B	24.14 ± 0.07	26.08 ± 0.37	0.755	0.059	1.363	0.139	0.66	3.84	1.75	1.08	2.85	2.17	270.92	276.79
		n = 8	C	24.22 ± 0.05	26.33 ± 0.31	0.871	0.075	1.742	0.197	0.77	3.75	1.65	1.31	2.74	1.97	278.72	283.25
		n = 9	D	24.29 ± 0.06	26.61 ± 0.60	0.871	0.095	1.963	0.219	0.79	3.73	1.68	1.55	2.46	2.07	263.31	269.98
		n = 10	E	24.30 ± 0.09	25.75 ± 0.24	0.877	0.045	1.630	0.142	0.78	3.90	1.66	1.27	2.97	1.98	261.00	265.38
		Mean		24.2 ± 0.14	26.17 ± 0.61	0.866	0.065	1.633	0.176	0.76	3.93	1.71	1.32	2.75	2.13	309.19	314.38
3	Crawling	n = 11	A	22.96 ± 0.01	23.23 ± 0.06	0.773	0.020	1.015	0.053	0.63	5.01	1.75	0.82	4.58	2.06	414.69	416.49
		n = 12	B	22.95 ± 0.01	23.77 ± 0.13	0.661	0.006	0.934	0.019	0.58	4.22	1.71	0.79	3.62	2.02	221.79	223.05
		n = 13	C	22.93 ± 0.01	24.24 ± 0.09	0.617	0.025	1.145	0.082	0.56	3.96	1.66	0.71	3.42	1.84	174.96	176.33
		n = 14	D	23.82 ± 0.08	28.18 ± 0.53	1.178	0.020	1.660	0.065	1.00	4.21	1.81	1.44	3.46	2.20	497.43	501.33
		n = 15	E	24.00 ± 0.08	28.35 ± 0.38	1.221	0.071	1.683	0.129	1.09	4.23	1.73	1.32	3.74	1.90	447.56	449.75
		Mean		23.3 ± 0.48	25.40 ± 2.25	0.890	0.028	1.288	0.070	0.80	4.40	1.80	1.00	3.71	2.00	351.29	353.39
4	Crawling	n = 16	A	24.13 ± 0.07	26.78 ± 0.68	0.592	0.010	0.918	0.028	0.39	4.08	1.72	0.63	3.27	2.13	441.52	443.58
		n = 17	B	24.26 ± 0.05	27.68 ± 0.48	0.439	0.035	0.655	0.089	0.27	4.97	1.72	0.43	4.16	2.34	384.86	386.97
		n = 18	C	24.36 ± 0.04	28.75 ± 0.69	0.474	0.048	0.737	0.088	0.28	3.95	1.60	0.48	3.18	1.98	385.68	387.85
		n = 19	D	24.41 ± 0.06	28.77 ± 0.37	0.502	0.030	0.696	0.075	0.28	4.67	1.87	0.57	3.94	3.23	503.03	504.83
		n = 20	E	24.50 ± 0.03	29.01 ± 0.24	0.430	0.037	0.647	0.075	0.26	4.70	1.89	0.45	3.64	2.64	402.42	404.30
		Mean		24.32 ± 0.14	28.10 ± 1.03	0.488	0.032	0.731	0.071	0.29	4.42	1.72	0.48	3.34	2.25	423.50	425.51
5	Crawling	n = 21	A	24.29 ± 0.08	26.51 ± 0.33	1.026	0.022	1.640	0.114	0.91	3.46	1.56	1.31	2.96	1.71	220.95	226.42
		n = 22	B	24.46 ± 0.05	27.37 ± 0.54	1.422	0.110	2.547	0.207	1.27	3.37	1.57	1.97	2.77	1.73	288.81	295.39
		n = 23	C	24.56 ± 0.05	28.05 ± 0.49	1.644	0.066	2.961	0.137	1.50	3.42	1.57	2.30	2.80	1.74	305.74	314.62
		n = 24	D	24.66 ± 0.05	28.37 ± 0.23	2.329	0.124	4.038	0.260	2.15	3.46	1.55	3.17	2.89	1.72	353.03	363.65
		n = 25	E	24.73 ± 0.04	27.93 ± 0.04	3.216	0.149	5.450	0.276	2.93	3.43	1.59	4.22	2.87	1.76	616.70	627.59
		Mean		24.52 ± 0.16	27.61 ± 0.79	1.928	0.094	3.327	0.199	1.63	3.43	1.57	2.24	2.86	1.73	357.04	365.53

Carpet	Movement	Test	Path	OPS										IOM Data		
								dN/dlogDp						Avg. PM_{100} (µg/m^3)		
								Mode 1			Mode 2					
				N_T (cm^{-3})	$N_{T,bgd}$ (cm^{-3})	Avg. $PM_{2.5}$ (µg/m^3)	Avg. PM_{10} (µg/m3)	A (cm^{-3})	D_{pg} (µm)	σ_g	A (cm^{-3})	D_{pg} (µm)	σ_g	Infant BZ	Adult BZ	Infant BZ/ Adult BZ
1	Crawling	n = 1	A	0.983	0.035	0.963	43.355	2.56	2.90	1.60	1.18	5.90	1.20	187.76	57.95	3.24
		n = 2	B	1.026	0.049	0.807	36.823	2.15	2.90	1.60	1.03	5.80	1.20			
		n = 3	C	0.891	0.050	0.739	28.241	1.87	2.80	1.60	0.80	5.80	1.20			
		n = 4	D	0.896	0.099	0.637	42.517	2.06	3.20	1.70	0.90	6.20	1.20			
		n = 5	E	0.801	0.054	0.470	24.872	1.36	3.00	1.60	0.64	5.90	1.20			
		Mean		0.919	0.057	0.715	34.279	1.87	2.87	1.57	0.96	5.89	1.20			
2	Crawling	n = 6	A	0.118	0.073	0.154	10.810	0.57	3.30	1.70	0.18	5.80	1.10	259.03	--	--
		n = 7	B	0.365	0.054	0.250	13.071	0.47	2.50	1.40	0.58	5.80	1.30			
		n = 8	C	0.559	0.062	0.425	19.773	1.06	2.70	1.60	0.84	6.40	1.30			
		n = 9	D	0.496	0.104	0.369	12.927	0.74	2.50	1.50	0.74	6.60	1.40			
		n = 10	E	0.348	0.061	0.256	14.323	1.08	3.80	1.80	0.21	5.90	1.10			
		Mean		0.377	0.071	0.291	14.181	0.77	2.87	1.60	0.43	6.02	1.22			
3	Crawling	n = 11	A	0.147	0.022	0.111	12.009	0.37	3.20	1.50	0.31	6.10	1.20	207.57	17.73	11.7
		n = 12	B	0.142	0.009	0.123	9.925	0.31	2.90	1.50	0.27	6.10	1.20			
		n = 13	C	0.548	0.034	0.290	10.609	0.38	2.20	1.40	0.71	6.10	1.40			
		n = 14	D	0.179	0.030	0.161	13.512	0.47	3.00	1.50	0.30	5.90	1.20			
		n = 15	E	0.216	0.060	0.193	17.840	0.86	3.70	1.80	0.28	5.90	1.10			
		Mean		0.247	0.031	0.175	12.779	0.47	2.96	1.60	0.36	6.03	1.22			
4	Crawling	n = 16	A	0.226	0.013	0.200	12.837	0.59	3.00	1.60	0.34	6.00	1.20	306.63	149.93	2.05
		n = 17	B	0.089	0.035	0.067	4.630	0.14	2.70	1.40	0.14	5.90	1.20			
		n = 18	C	0.136	0.033	0.110	7.829	0.34	3.00	1.70	0.15	6.20	1.20			
		n = 19	D	0.234	0.037	0.170	19.901	0.51	3.20	1.60	0.44	6.10	1.20			
		n = 20	E	0.199	0.039	0.158	14.011	0.42	3.10	1.60	0.34	6.10	1.20			
		Mean		0.177	0.031	0.141	11.842	0.37	2.92	1.53	0.32	6.10	1.22			
5	Crawling	n = 21	A	0.688	0.051	0.783	43.342	2.27	3.00	1.50	1.38	5.80	1.20	86.76	67.79	1.28
		n = 22	B	0.935	0.076	1.100	47.959	2.99	2.90	1.50	1.59	5.80	1.20			
		n = 23	C	1.399	0.060	1.578	72.060	4.20	2.90	1.50	2.38	5.80	1.20			
		n = 24	D	1.754	0.113	2.014	90.030	5.09	2.80	1.50	4.39	6.20	1.30			
		n = 25	E	2.212	0.113	2.623	114.169	7.08	2.90	1.50	3.98	5.90	1.20			
		Mean		1.398	0.082	1.508	68.995	3.76	2.80	1.48	3.06	5.97	1.27			

Carpet	Movement	Test	Path	Temperature (°C) (mean ± standard deviation)	Relative Humidity (%) (mean ± standard deviation)	BioScout											
						N_F (cm^{-3})	$N_{F,bgd}$ (cm^{-3})	N_T (cm^{-3})	$N_{T,bgd}$ (cm^{-3})	$dN_F/dlogDp$ $Mode_{FBAP}$			$dN_T/dlogDp$ $Mode_{Total}$			M_F (μg m^{-3})	M_T (μg m^{-3})
										A (cm^{-3})	D_{pg} (μm)	σ_g	A (cm^{-3})	D_{pg} (μm)	σ_g		
1	Walking	n = 26	A	24.26 ± 0.04	21.43 ± 0.33	1.601	0.016	3.952	0.037	1.53	3.18	1.52	2.79	2.38	1.73	149.36	156.47
		n = 27	B	24.43 ± 0.04	22.05 ± 0.44	0.970	0.150	2.592	0.375	0.93	3.29	1.51	1.88	2.30	1.80	88.44	94.67
		n = 28	C	24.45 ± 0.02	21.64 ± 0.38	0.864	0.030	2.036	0.096	0.84	3.23	1.56	1.39	2.49	1.75	100.59	103.99
		n = 29	D	24.59 ± 0.02	21.76 ± 0.34	0.564	0.038	1.227	0.125	0.52	3.30	1.51	0.84	2.65	1.69	62.84	65.27
		n = 30	E	24.61 ± 0.03	21.49 ± 0.27	0.726	0.070	1.629	0.166	0.71	3.51	1.60	1.27	2.52	1.87	95.40	99.09
		Mean		24.47 ± 0.13	21.67 ± 0.41	0.945	0.061	2.287	0.160	0.92	3.27	1.55	1.65	2.42	1.78	99.33	103.90
2	Walking	n = 31	A	23.95 ± 0.07	16.02 ± 0.38	--	--	--	--	--	--	--	--	--	--	--	
		n = 32	B	24.07 ± 0.2	16.46 ± 0.60	0.841	0.071	1.876	0.146	0.75	3.35	1.60	1.31	2.50	1.87	167.53	171.06
		n = 33	C	24.14 ± 0.02	16.43 ± 0.46	0.876	0.099	1.784	0.239	0.83	3.50	1.64	1.38	2.61	1.93	150.09	153.81
		n = 34	D	24.20 ± 0.03	16.38 ± 0.34	1.169	0.142	2.564	0.306	1.02	3.43	1.66	1.82	2.42	2.00	292.15	297.38
		n = 35	E	24.31 ± 0.03	16.23 ± 0.12	0.824	0.171	1.639	0.386	0.78	3.32	1.65	1.30	2.49	1.88	156.94	162.19
		Mean		24.13 ± 0.13	16.30 ± 0.43	0.927	0.121	1.966	0.269	0.86	3.41	1.66	1.45	2.50	1.93	191.68	196.11
3	Walking	n = 36	A	24.32 ± 0.07	30.26 ± 0.70	0.496	0.004	0.746	0.014	0.45	3.47	1.61	0.61	3.04	1.74	86.79	88.65
		n = 37	B	24.51 ± 0.05	30.92 ± 0.48	0.647	0.052	1.056	0.093	0.60	3.31	1.54	0.81	2.89	1.71	59.54	61.20
		n = 38	C	24.62 ± 0.07	30.79 ± 0.27	0.454	0.095	0.659	0.165	0.46	3.50	1.77	0.58	3.02	1.86	73.95	75.05
		n = 39	D	24.66 ± 0.03	30.84 ± 0.39	0.673	0.058	1.110	0.095	0.65	3.25	1.61	0.89	2.76	1.78	76.25	77.94
		n = 40	E	24.72 ± 0.03	31.16 ± 0.44	0.836	0.062	1.384	0.114	0.83	3.33	1.60	1.15	2.80	1.73	83.64	86.10
		Mean		24.57 ± 0.15	30.79 ± 0.54	0.621	0.054	0.991	0.096	0.60	3.37	1.63	0.82	2.86	1.78	76.03	77.79
4	Walking	n = 41	A	24.09 ± 0.05	19.07 ± 0.20	0.199	0.028	0.346	0.078	0.19	4.05	1.72	0.30	3.03	1.98	49.83	50.85
		n = 42	B	24.26 ± 0.05	19.11 ± 0.50	0.175	0.031	0.353	0.077	0.14	3.67	1.58	0.27	2.68	1.94	59.17	60.65
		n = 43	C	24.31 ± 0.04	18.93 ± 0.47	0.166	0.036	0.337	0.085	0.14	3.94	1.54	0.23	3.10	1.92	41.70	42.68
		n = 44	D	24.44 ± 0.02	18.92 ± 0.73	0.181	0.010	0.386	0.023	0.16	4.06	1.54	0.28	3.02	1.92	42.32	43.39
		n = 45	E	24.54 ± 0.02	20.23 ± 0.62	0.461	0.043	0.850	0.098	0.42	3.70	1.62	0.65	2.91	1.78	113.95	116.26
		Mean		24.33 ± 0.16	19.25 ± 0.71	0.236	0.030	0.454	0.072	0.20	3.78	1.57	0.35	2.92	1.88	61.40	62.77
5	Walking	n = 46	A	24.48 ± 0.06	28.21 ± 0.39	0.909	0.027	1.699	0.086	0.88	3.07	1.58	1.36	2.52	1.73	91.55	95.27
		n = 47	B	24.55 ± 0.03	28.21 ± 0.53	1.359	0.109	2.223	0.214	1.30	3.31	1.52	1.86	2.81	1.65	115.01	119.42
		n = 48	C	24.55 ± 0.04	28.82 ± 0.18	1.732	0.126	2.945	0.215	1.69	3.26	1.57	2.41	2.74	1.69	131.04	136.89
		n = 49	D	24.67 ± 0.04	28.30 ± 0.16	1.778	0.244	3.071	0.434	1.68	3.27	1.49	2.30	2.86	1.58	127.24	134.05
		n = 50	E	24.80 ± 0.01	28.62 ± 0.28	1.424	0.229	2.617	0.376	1.42	3.17	1.55	2.06	2.64	1.67	86.10	90.86
		Mean		24.61 ± 0.12	28.67 ± 0.54	1.440	0.147	2.511	0.265	1.40	3.23	1.54	1.93	2.79	1.64	110.19	115.30

Carpet	Movement	Test	Path	OPS										IOM Data		
								dN/dlogDp						Avg. PM_{100} ($\mu g/m^3$)		
								Mode 1			Mode 2					
				N_T (cm^{-3})	$N_{T,bgd}$ (cm^{-3})	Avg. $PM_{2.5}$ ($\mu g/m^3$)	Avg. PM_{10} ($\mu g/m^3$)	A (cm^{-3})	D_{pg} (μm)	σ_g	A (cm^{-3})	D_{pg} (μm)	σ_g	Infant BZ	Adult BZ	Infant BZ/ Adult BZ
1	Walking	n = 26	A	2.119	0.057	2.589	54.665	5.30	2.50	1.50	2.97	5.80	1.30	21.96	52.50	0.42
		n = 27	B	1.450	0.316	1.771	34.254	4.06	2.60	1.60	1.16	5.80	1.20			
		n = 28	C	1.103	0.130	1.315	30.170	2.65	2.50	1.50	1.54	5.90	1.30			
		n = 29	D	0.646	0.157	0.761	20.760	1.62	2.60	1.50	0.71	5.70	1.20			
		n = 30	E	0.888	0.164	1.058	26.842	2.57	2.70	1.60	0.89	5.80	1.20			
		Mean		1.241	0.165	1.499	33.338	3.24	2.58	1.53	1.34	5.73	1.22			
2	Walking	n = 31	A	0.673	0.288	0.737	32.449	1.82	2.80	1.50	1.08	5.90	1.20	52.04	37.90	1.37
		n = 32	B	0.989	0.241	1.113	37.335	2.67	2.70	1.60	1.19	5.90	1.20			
		n = 33	C	0.984	0.271	1.077	39.565	2.76	2.80	1.60	1.18	5.90	1.20			
		n = 34	D	0.959	0.362	1.072	38.676	2.68	2.80	1.60	1.25	5.80	1.20			
		n = 35	E	0.850	0.413	0.951	38.862	2.12	2.70	1.50	1.36	5.80	1.20			
		Mean		0.891	0.315	0.990	37.377	2.54	2.83	1.59	1.07	5.87	1.18			
3	Walking	n = 36	A	0.324	0.212	0.393	17.628	1.07	2.90	1.50	0.65	5.90	1.20	68.52	35.80	1.91
		n = 37	B	0.501	0.103	0.614	23.078	1.55	2.80	1.50	0.85	5.80	1.20			
		n = 38	C	0.266	0.178	0.304	17.783	1.12	3.30	1.60	0.50	6.10	1.20			
		n = 39	D	0.538	0.120	0.647	23.198	1.67	2.80	1.50	0.91	5.80	1.20			
		n = 40	E	0.716	0.131	0.896	32.782	2.36	2.90	1.50	1.15	5.90	1.20			
		Mean		0.469	0.149	0.571	22.894	1.55	2.90	1.52	0.86	5.92	1.22			
4	Walking	n = 41	A	0.174	0.028	0.188	9.484	0.47	2.80	1.50	0.33	5.80	1.20	27.03	17.03	1.59
		n = 42	B	0.180	0.039	0.158	6.552	0.42	2.80	1.60	0.22	5.70	1.20			
		n = 43	C	0.210	0.036	0.161	8.049	0.44	2.90	1.60	0.25	5.90	1.20			
		n = 44	D	0.317	0.008	0.183	9.543	0.51	3.00	1.60	0.29	5.90	1.20			
		n = 45	E	0.487	0.045	0.500	21.081	1.22	2.80	1.50	0.68	5.80	1.20			
		Mean		0.274	0.031	0.238	10.942	0.67	2.95	1.59	1.09	5.82	1.17			
5	Walking	n = 46	A	0.739	0.040	1.055	28.942	2.66	2.80	1.50	1.11	5.80	1.20	78.56	69.95	1.12
		n = 47	B	1.050	0.089	1.233	50.745	3.67	3.00	1.50	1.99	5.90	1.20			
		n = 48	C	1.459	0.094	1.719	64.747	4.81	2.90	1.50	2.48	5.80	1.20			
		n = 49	D	1.521	0.169	1.965	62.614	4.11	2.60	1.40	3.95	5.70	1.30			
		n = 50	E	1.374	0.150	1.699	49.064	4.26	2.80	1.50	2.06	5.70	1.20			
		Mean		0.916	0.109	1.534	51.223	3.35	2.64	1.42	3.17	5.79	1.31			

Notes:

N_F: Averaged size-integrated (0.4-15.4 μm) FBAP number concentration measured during the 20-minute resuspension periods.

N_T: Averaged size-integrated (0.4-15.4 μm for the BioScout, 1-11.2 μm for the OPS) total particle number concentration measured during the 20-minute resuspension periods.

$N_{F,bgd}$: Averaged size-integrated (0.4-15.4 μm) FBAP number concentration measured during the 10 minute background periods.

$N_{T,bgd}$: Averaged size-integrated (0.4-15.4 μm for the BioScout, 1-11.2 μm for the OPS) total particle number concentration measured during the 10 minute background periods.

M_F: Averaged size-integrated (0.4-15.4 μm) FBAP mass concentration measured during the 20-minute resuspension periods.

M_T: Averaged size-integrated (0.4-15.4 μm for the BioScout) total particle mass concentration measured during the 20-minute resuspension periods.

$dN/dlogD_p$: Lognormal fitting parameters of the mean number concentration size distribution measured during the resuspension periods, including amplitude (A), modal diameter (D_{pg}), and standard deviation (σ_g).

Avg. $PM_{2.5}$: Averaged particle mass concentration (< 2.5 μm) measured during the 20-minute resuspension periods, from OPS (ρ_{eff}=1.204 g cm^{-3}).

Avg. PM_{10}: Averaged particle mass concentration (< 10 μm) measured during the 20-minute resuspension periods, from OPS (ρ_{eff}=1.204 g cm^{-3}).

Avg. PM100: Averaged particle mass concentration (< 100 μm) over all five paths on each carpet measured during the resuspension periods (100 minute in total), from IOM.

Table S5. Statistical analysis (p-values) of the comparisons of N_F, M_F, and $RTDDR_F$ between different activity patterns, carpets, and breathing routes.

			Activity Patterns: Crawling and walking		
BioScout: N_F (N=25)			**0.039**		
BioScout: M_F (N=25)			**<0.001**		
$RTDDR_F$ – Total (N=5)			0.095		
$RTDDR_F$ – Head (N=5)			**0.032**		
$RTDDR_F$ – Tracheobronchial (N=5)			0.056		
$RTDDR_F$ – Pulmonary (N=5)			0.095		
Weight-Normalized $RTDDR_F$ – Total (N=5)			**0.016**		
Weight-Normalized $RTDDR_F$ – Head (N=5)			0.151		
Weight-Normalized $RTDDR_F$ – Tracheobronchial (N=5)			**0.008**		
Weight-Normalized $RTDDR_F$ – Pulmonary (N=5)			0.095		
			Breathing Routes: Nasal & Oral		
$RTDDR_F$-Total (N=5)			0.548		
$RTDDR_F$-Head (N=5)			0.095		
$RTDDR_F$-Tracheobronchial (N=5)			0.548		
$RTDDR_F$-Pulmonary (N=5)			0.421		
N_F – Crawling (for each p-value, N=5)					
	Carpet 1	Carpet 2	Carpet 3	Carpet 4	Carpet 5
Carpet 1	--	**0.008**	**0.008**	**0.008**	0.421
Carpet 2	--	--	0.841	**0.008**	**0.008**
Carpet 3	--	--	--	**0.008**	**0.032**
Carpet 4	--	--	--	--	**0.008**
N_F – Walking (for each p-value, N=5)					
	Carpet 1	Carpet 2	Carpet 3	Carpet 4	Carpet 5
Carpet 1	--	0.841	0.095	**0.008**	0.095
Carpet 2	--	--	0.222	0.151	**0.016**
Carpet 3	--	--	--	**0.016**	**0.008**
Carpet 4	--	--	--	--	**0.008**
M_F – Crawling (for each p-value, N=5)					
	Carpet 1	Carpet 2	Carpet 3	Carpet 4	Carpet 5
Carpet 1	--	**0.032**	0.310	0.310	0.095
Carpet 2	--	--	1	0.095	0.421
Carpet 3	--	--	--	0.841	1
Carpet 4	--	--	--	--	0.151
M_F – Walking (for each p-value, N=5)					
	Carpet 1	Carpet 2	Carpet 3	Carpet 4	Carpet 5
Carpet 1	--	0.151	0.095	0.095	0.690
Carpet 2	--	--	0.151	0.151	0.151
Carpet 3	--	--	--	0.151	**0.016**
Carpet 4	--	--	--	--	**0.032**

N=sample size

Table S6. Statistical analysis of the comparisons between LIF and qPCR presented in Figure S7.

	BioScout: FBAP Number Concentration*			
	Crawling		Walking	
	Correlation Coefficient	*p*-value	Correlation Coefficient	*p*-value
qPCR: Total Bacterial & Fungal Concentration in Air	-0.550	**0.021**	0.021	**0.014**
qPCR: Total Bacterial & Fungal Concentration in Carpet Dust	-0.160	0.065	0.093	0.065
PAMAS: Total Particle Number Concentration (>1 μm) in Carpet Dust	0.344	0.134	0.828	0.134
Dust Load	-0.308	**0.019**	0.179	**0.014**
	BioScout: Total Particle Number Concentration			
	Crawling		Walking	
	Correlation Coefficient	*p*-value	Correlation Coefficient	*p*-value
qPCR: Total Bacterial & Fungal Concentration in Air	-0.492	**0.030**	0.142	**0.014**
	PAMAS: Total Particle Number Concentration (>1 μm) in Carpet Dust			
	Correlation Coefficient		*p*-value	
qPCR: Total Bacterial & Fungal Concentration in Carpet Dust	-0.210		0.196	

*For each correlation coefficient or *p*-value, the sample size (*N*) = 5.

Figures

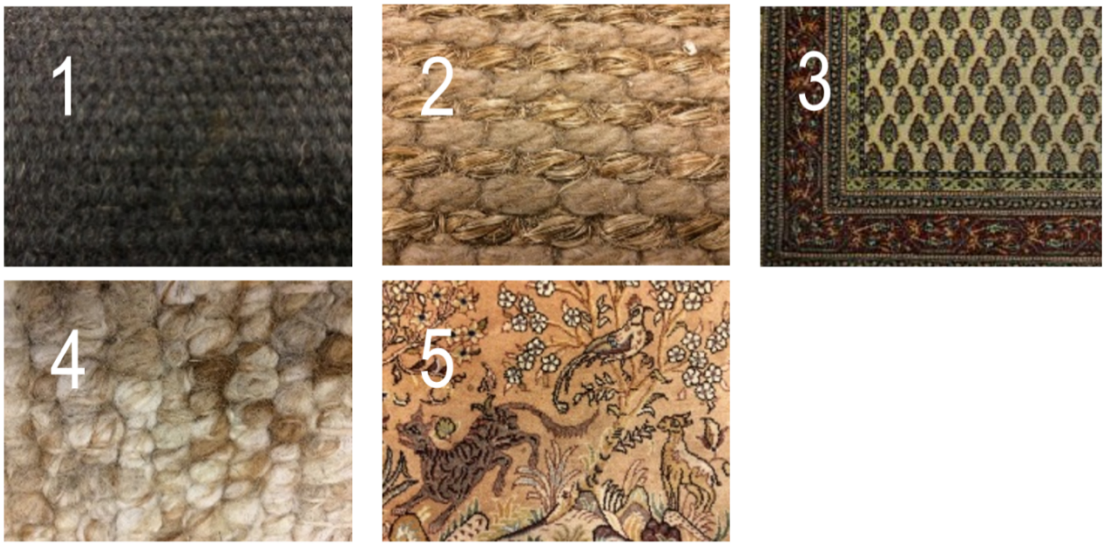

Figure S1. Photos of the five tested carpets, 1-5.

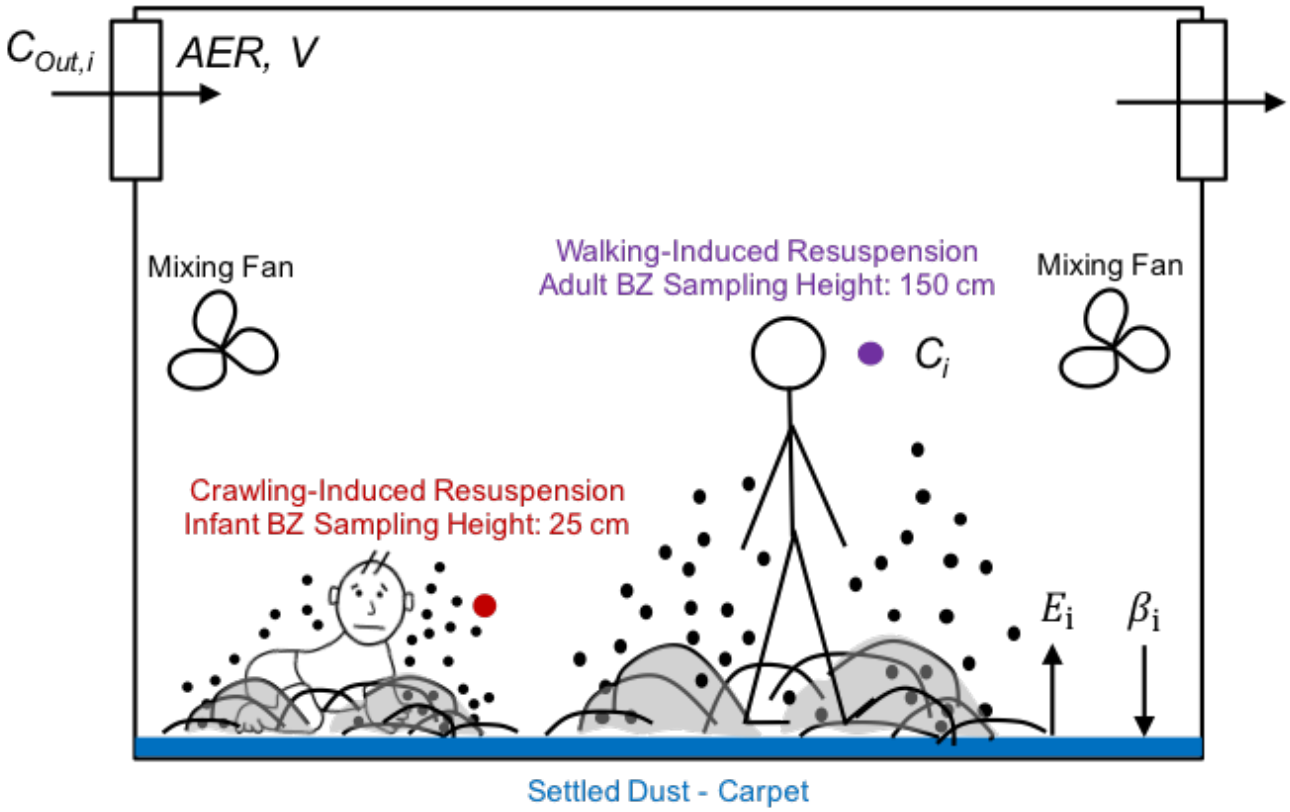

Figure S2. Schematic of chamber setup and material balance model parameters for estimating the size-resolved FBAP emission rates during adult walking resuspension events.

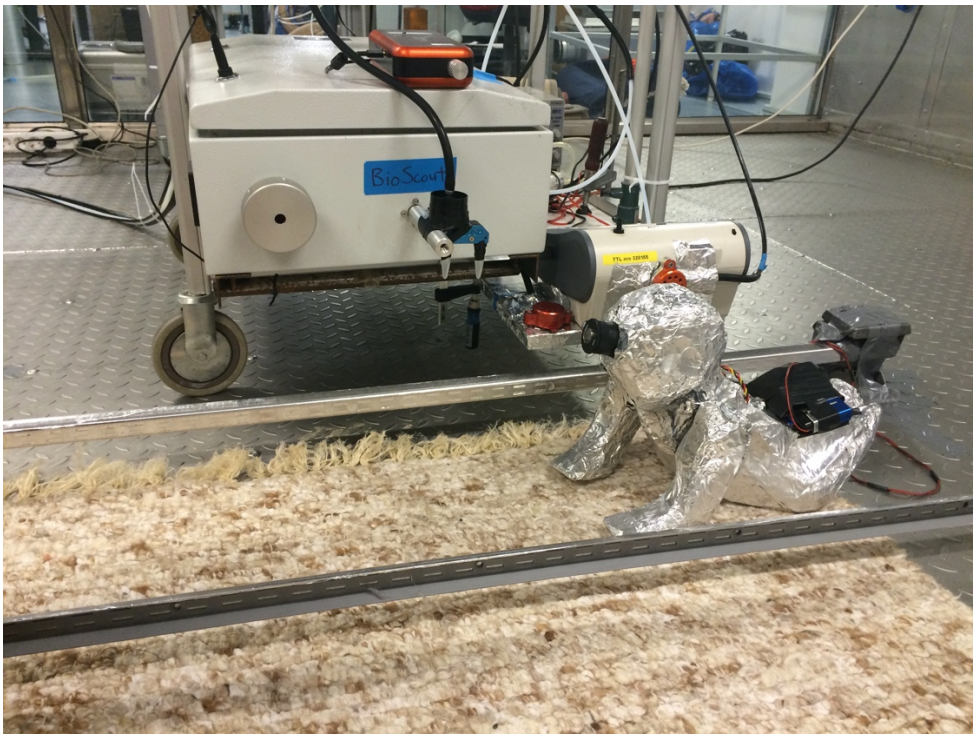

Figure S3. Photo of simplified mechanical crawling infant with mobile aerosol sampling (BioScout and OPS) on a mobile trolley in the infant breathing zone. Note: the OPS inlet was recessed 10 cm back from the crawling path.

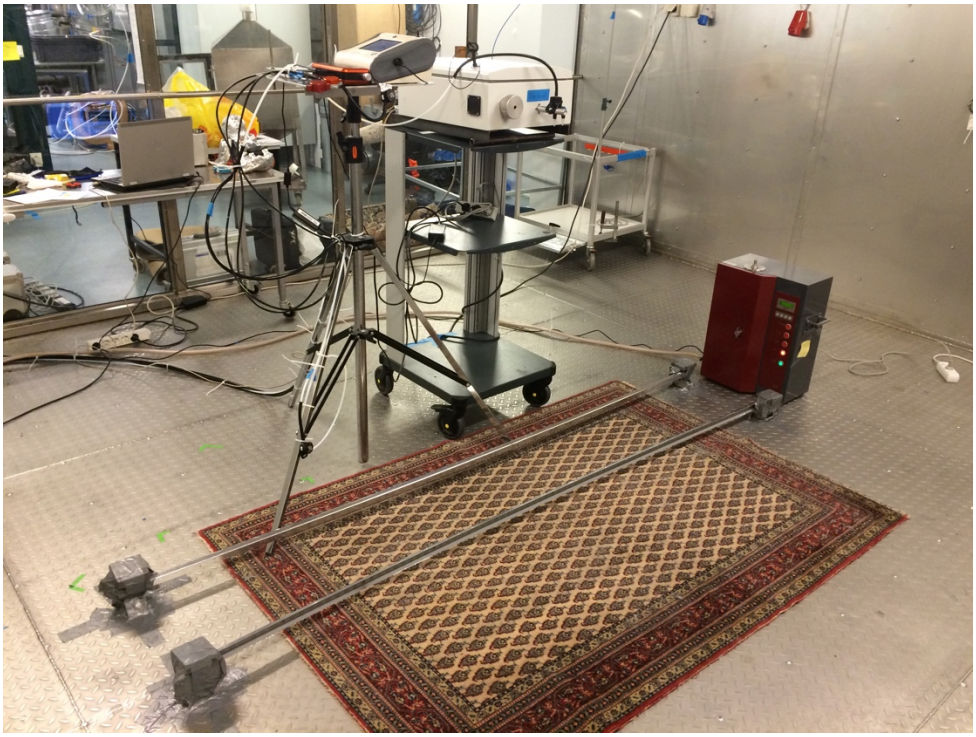

Figure S4. Photo of chamber setup with aerosol sampling (BioScout and OPS) in the adult breathing zone.

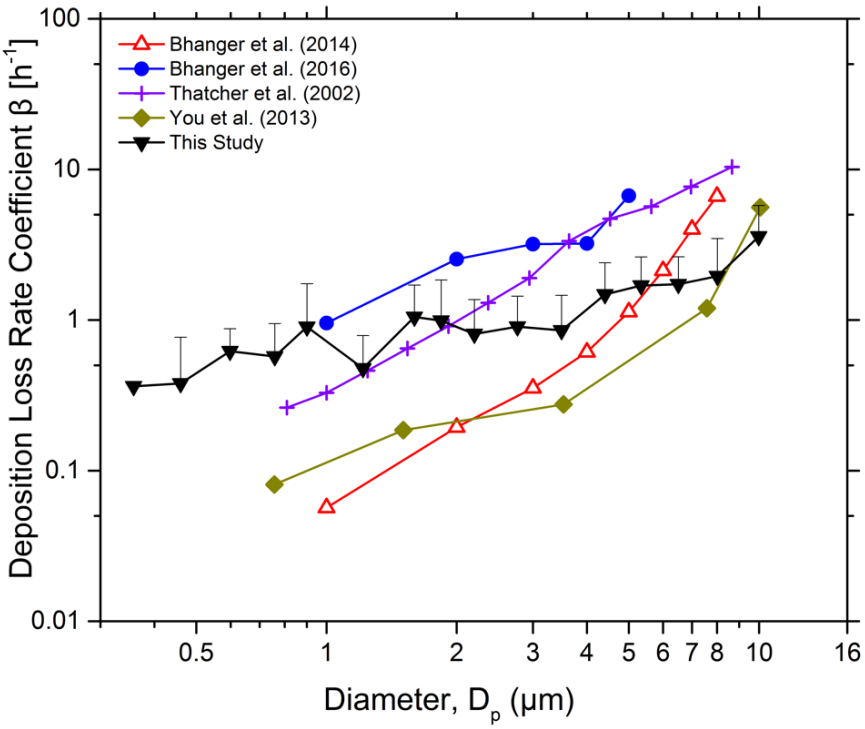

Figure S5. FBAP first-order deposition loss rate coefficients (β_i, h^{-1}) measured during the 10 minute decay periods of the adult walking experiments. FBAP deposition loss rate coefficients from Bhangar et al. (3) and Bhangar et al. (4) and total particle deposition loss rate coefficients from Thatcher et al. (72) and You et al. (85) are shown for comparison.

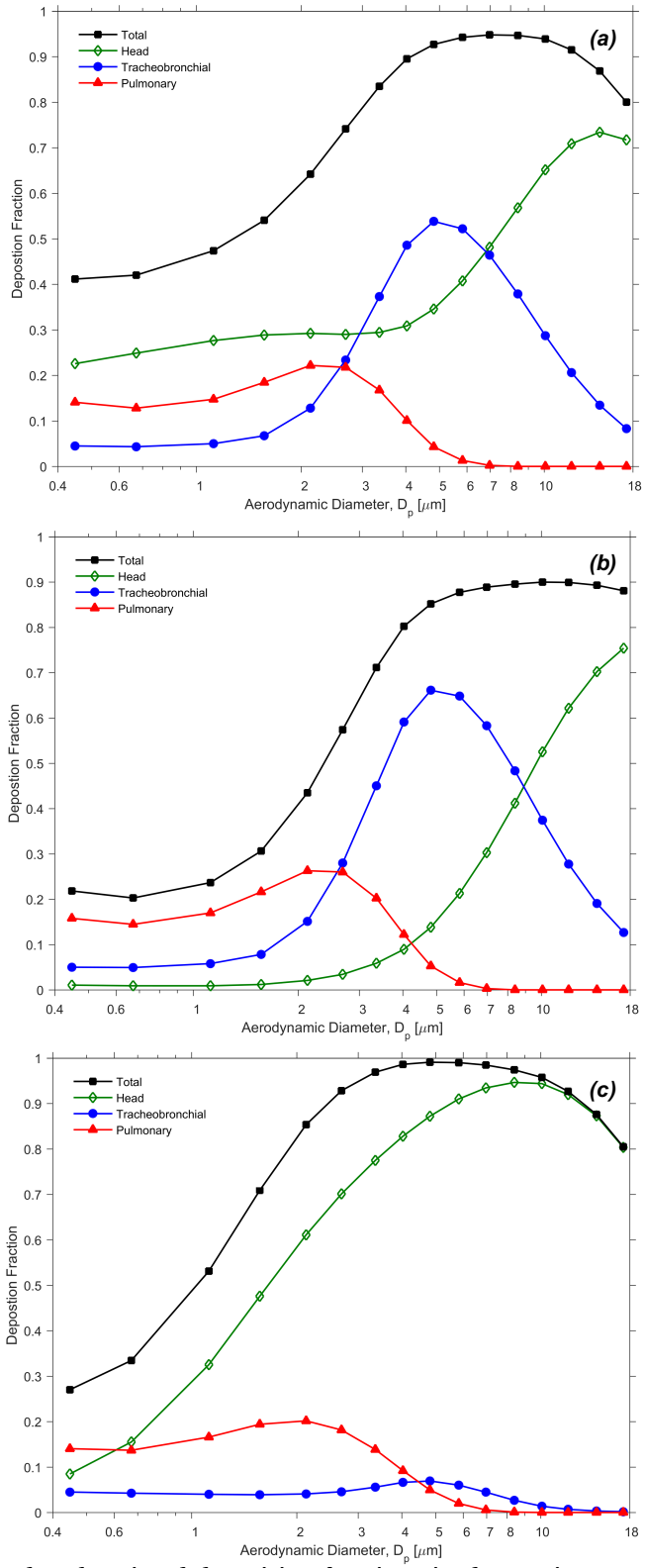

Figure S6. Size-resolved total and regional deposition fractions in the respiratory system for an extended size range up to 18 μm to match the hygroscopic-growth shifted FBAP size distributions in the infant and adult BZ (Figure S12): (a.) a 3-month old infant, nasal breathing route, (b.) a 3-month old infant, oral breathing route, and (c.) a 21-year old adult, nasal breathing route, obtained from the Multiple-Path Particle Dosimetry (MPPD) Model for breathing parameters stated in the Materials and Methods section.

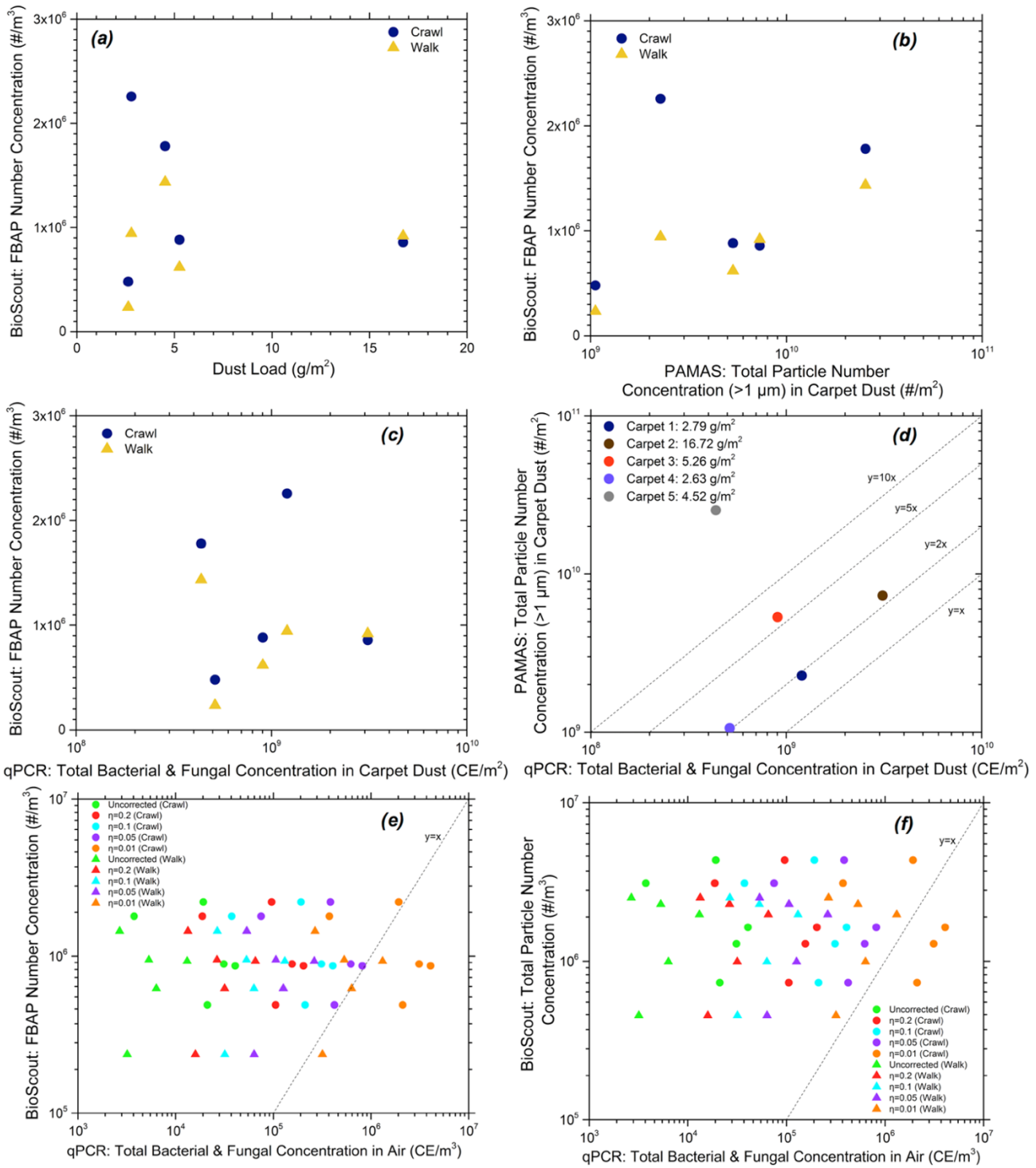

Figure S7. *Comparison between size-integrated (1-15.4 μm) FBAP number concentrations, as measured by the BioScout during both crawling and walking, with: (a.) sieved gravimetric carpet dust loads (pore size 1 mm x 1 mm), (b.) total particle number concentrations in carpet dust (>1 μm) via PAMAS, and (c.) total bacterial and fungal concentrations in carpet dust via qPCR (Hyytiäinen et al. (34)); (d.) comparison between total particle number concentrations in carpet dust (>1 μm) via PAMAS with total bacterial and fungal concentrations in carpet dust via qPCR; comparison between (e.) size-integrated (1-15.4 μm) FBAP and (f.) total particle number concentrations, as measured by the BioScout, with total bacterial and fungal concentrations in the infant and adult BZ via qPCR (Hyytiäinen et al. (34)), for a range of possible overall DNA and filter extraction efficiencies (η), informed by Hospodsky et al. (29). Note: 1 μm is used here as the lower size-cutoff for the BioScout data to match the PAMAS data.*

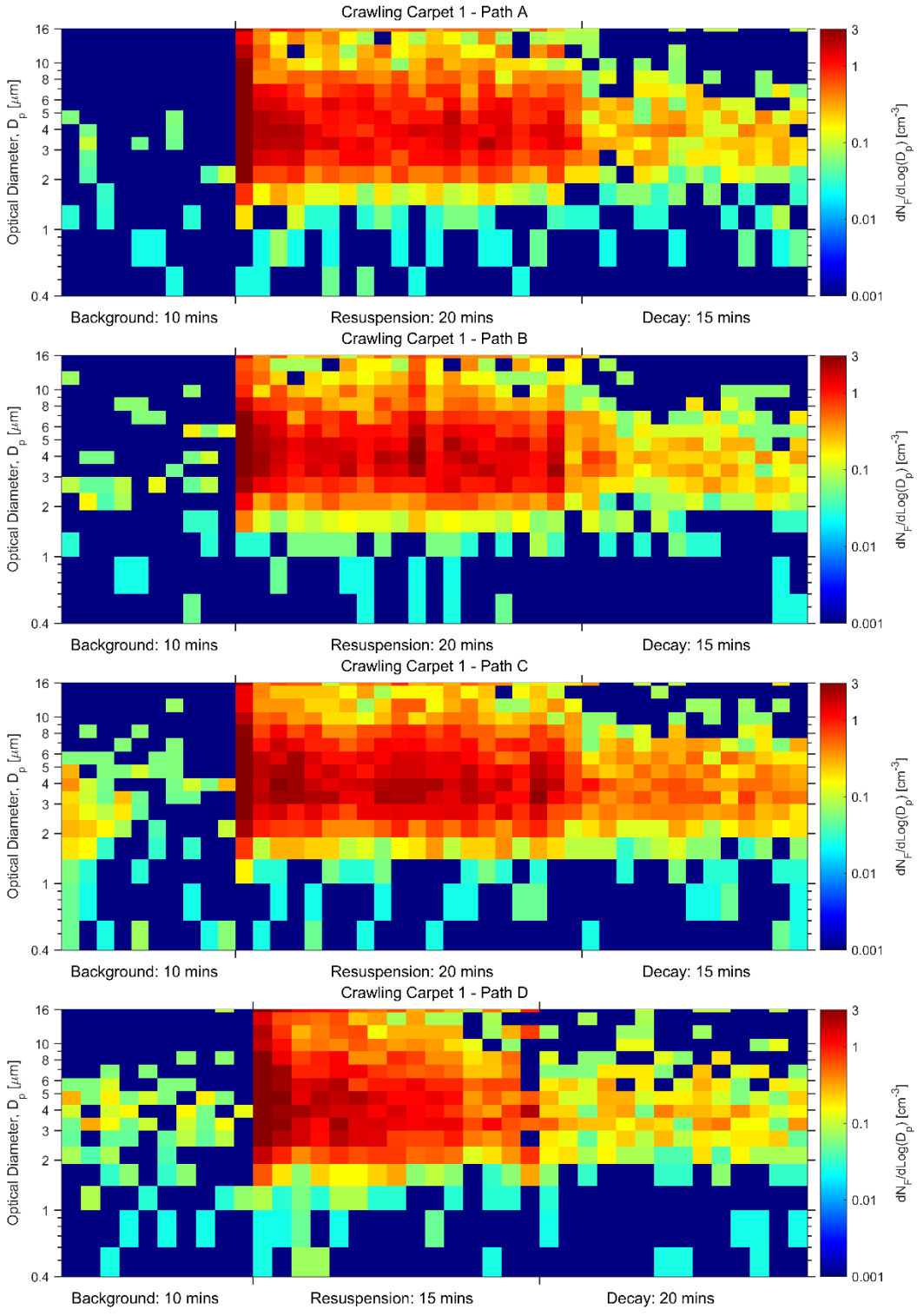
Crawling Carpet 1 - Path A
Optical Diameter, D_p [μm]
16
10
8
6
5
4
3
2
1
0.4
Background: 10 mins
Resuspension: 20 mins
Decay: 15 mins
3
1
0.1
0.01
0.001
$dN_F/dLog(D_p)$ [cm^{-3}]
Crawling Carpet 1 - Path B
Optical Diameter, D_p [μm]
Background: 10 mins
Resuspension: 20 mins
Decay: 15 mins
$dN_F/dLog(D_p)$ [cm^{-3}]
Crawling Carpet 1 - Path C
Optical Diameter, D_p [μm]
Background: 10 mins
Resuspension: 20 mins
Decay: 15 mins
$dN_F/dLog(D_p)$ [cm^{-3}]
Crawling Carpet 1 - Path D
Optical Diameter, D_p [μm]
Background: 10 mins
Resuspension: 15 mins
Decay: 20 mins
$dN_F/dLog(D_p)$ [cm^{-3}]

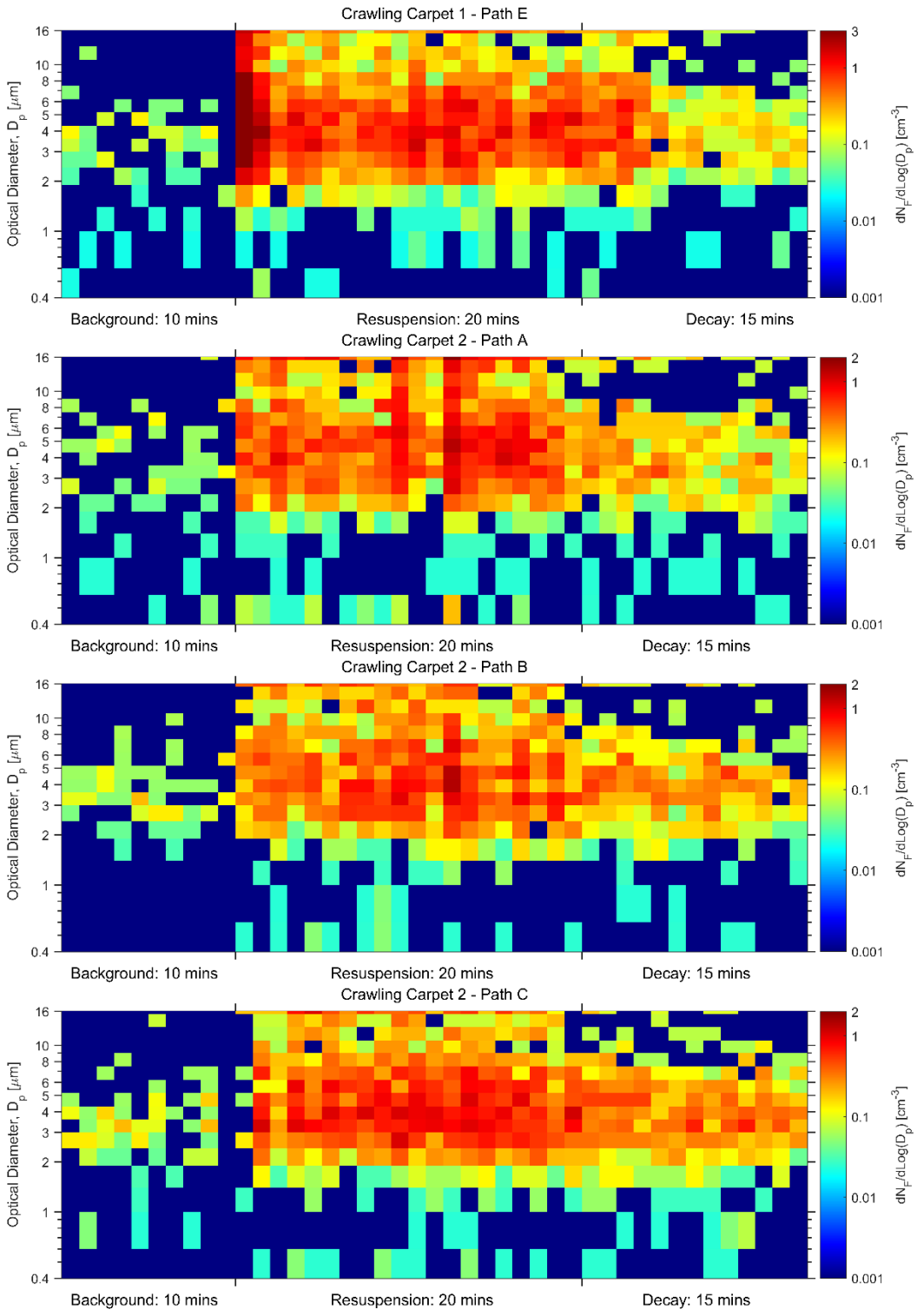
Crawling Carpet 1 - Path E
Crawling Carpet 2 - Path A
Crawling Carpet 2 - Path B
Crawling Carpet 2 - Path C
Optical Diameter, D_p [μm]
$dN_F/dLog(D_p)$ [cm^{-3}]
Background: 10 mins
Resuspension: 20 mins
Decay: 15 mins

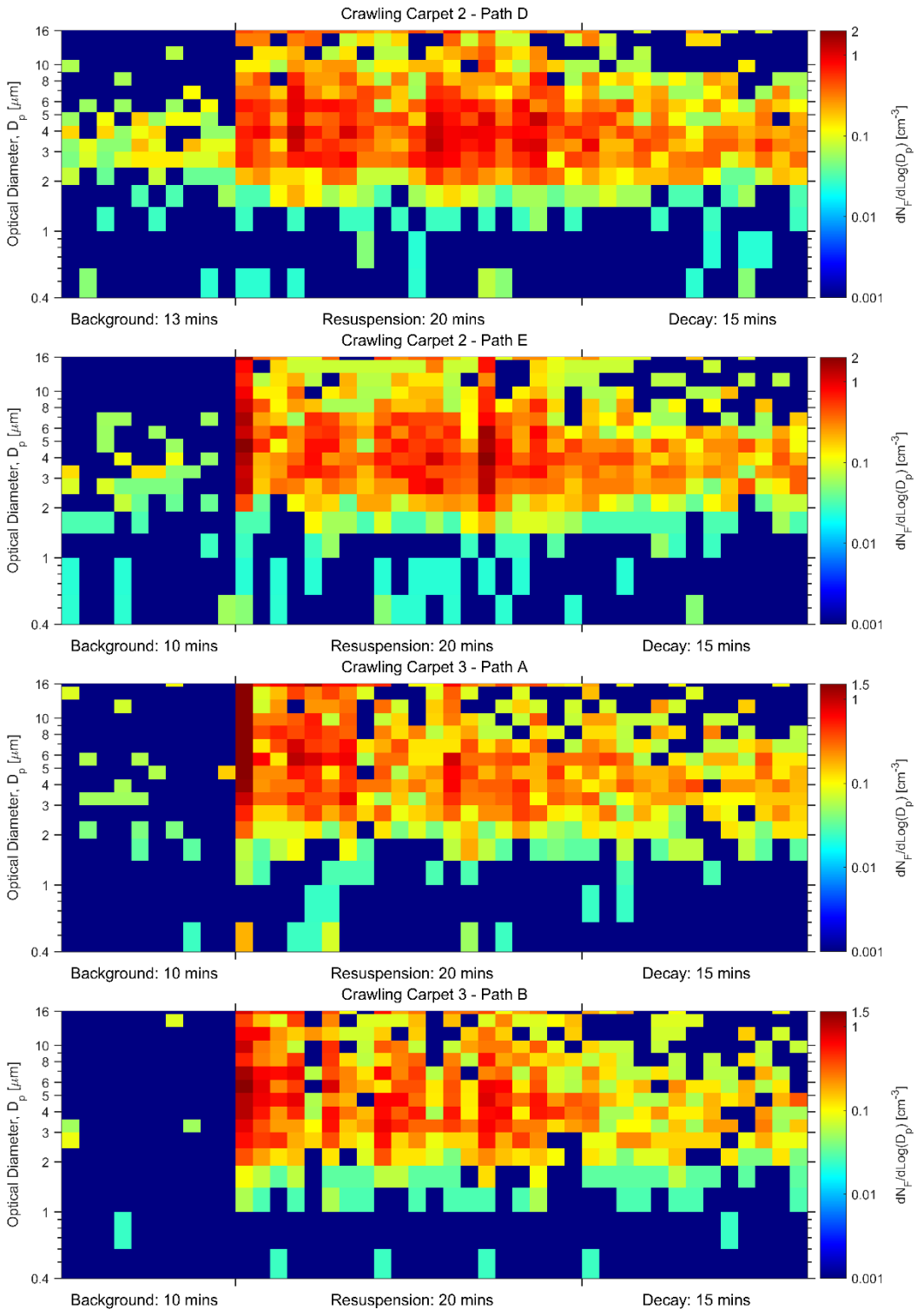
Crawling Carpet 2 - Path D
Optical Diameter, D_p [μm]
16
10
8
6
5
4
3
2
1
0.4
Background: 13 mins
Resuspension: 20 mins
Decay: 15 mins
2
1
0.1
0.01
0.001
$dN_F/dLog(D_p)$ [cm^{-3}]
Crawling Carpet 2 - Path E
Optical Diameter, D_p [μm]
Background: 10 mins
Resuspension: 20 mins
Decay: 15 mins
$dN_F/dLog(D_p)$ [cm^{-3}]
Crawling Carpet 3 - Path A
Optical Diameter, D_p [μm]
Background: 10 mins
Resuspension: 20 mins
Decay: 15 mins
1.5
1
0.1
0.01
0.001
$dN_F/dLog(D_p)$ [cm^{-3}]
Crawling Carpet 3 - Path B
Optical Diameter, D_p [μm]
Background: 10 mins
Resuspension: 20 mins
Decay: 15 mins
$dN_F/dLog(D_p)$ [cm^{-3}]

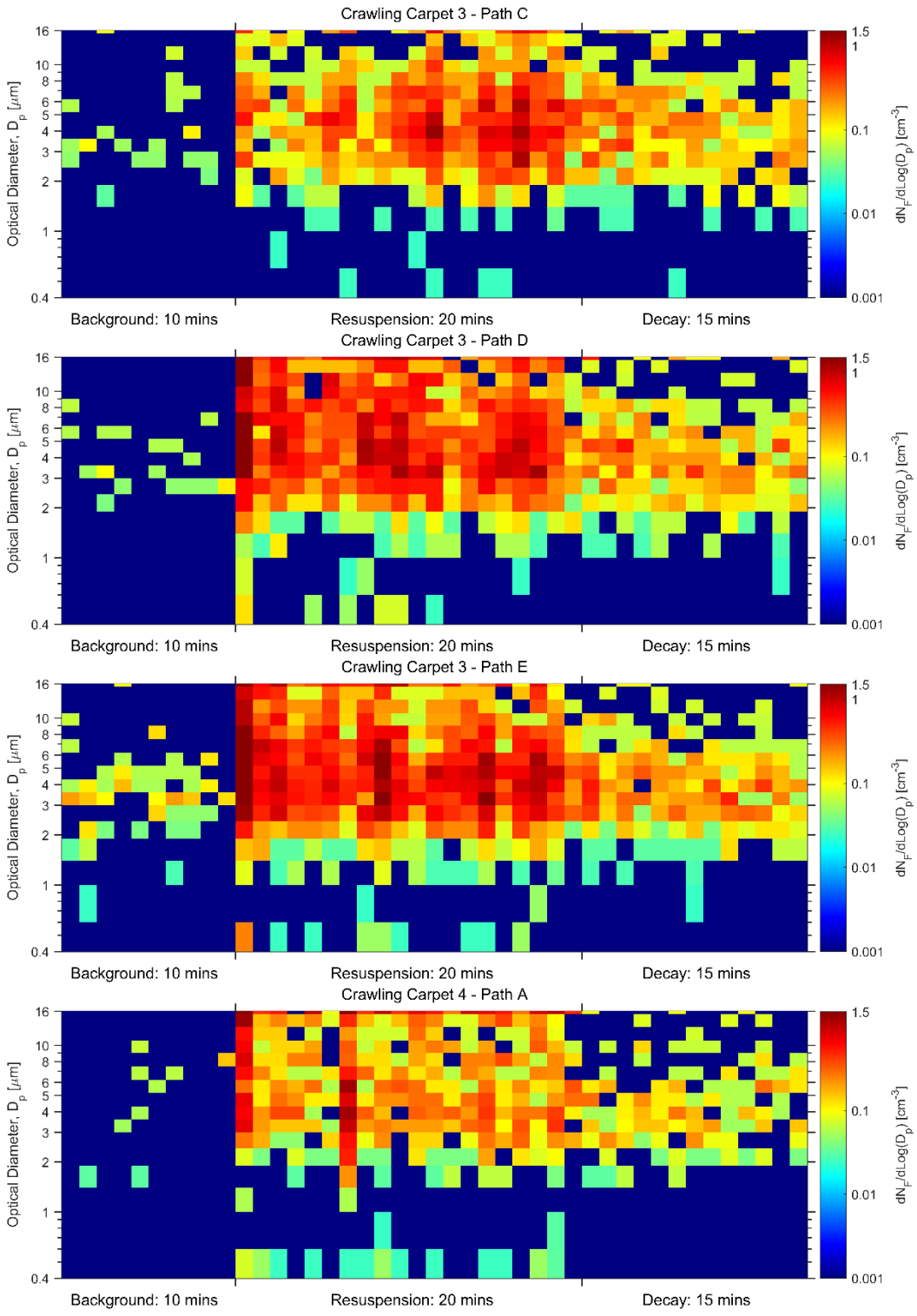
Crawling Carpet 3 - Path C
Optical Diameter, D_p [μm]
16
10
8
6
5
4
3
2
1
0.4
Background: 10 mins
Resuspension: 20 mins
Decay: 15 mins
1.5
1
0.1
0.01
0.001
$dN_F/dLog(D_p)$ [cm^{-3}]
Crawling Carpet 3 - Path D
Optical Diameter, D_p [μm]
Background: 10 mins
Resuspension: 20 mins
Decay: 15 mins
$dN_F/dLog(D_p)$ [cm^{-3}]
Crawling Carpet 3 - Path E
Optical Diameter, D_p [μm]
Background: 10 mins
Resuspension: 20 mins
Decay: 15 mins
$dN_F/dLog(D_p)$ [cm^{-3}]
Crawling Carpet 4 - Path A
Optical Diameter, D_p [μm]
Background: 10 mins
Resuspension: 20 mins
Decay: 15 mins
$dN_F/dLog(D_p)$ [cm^{-3}]

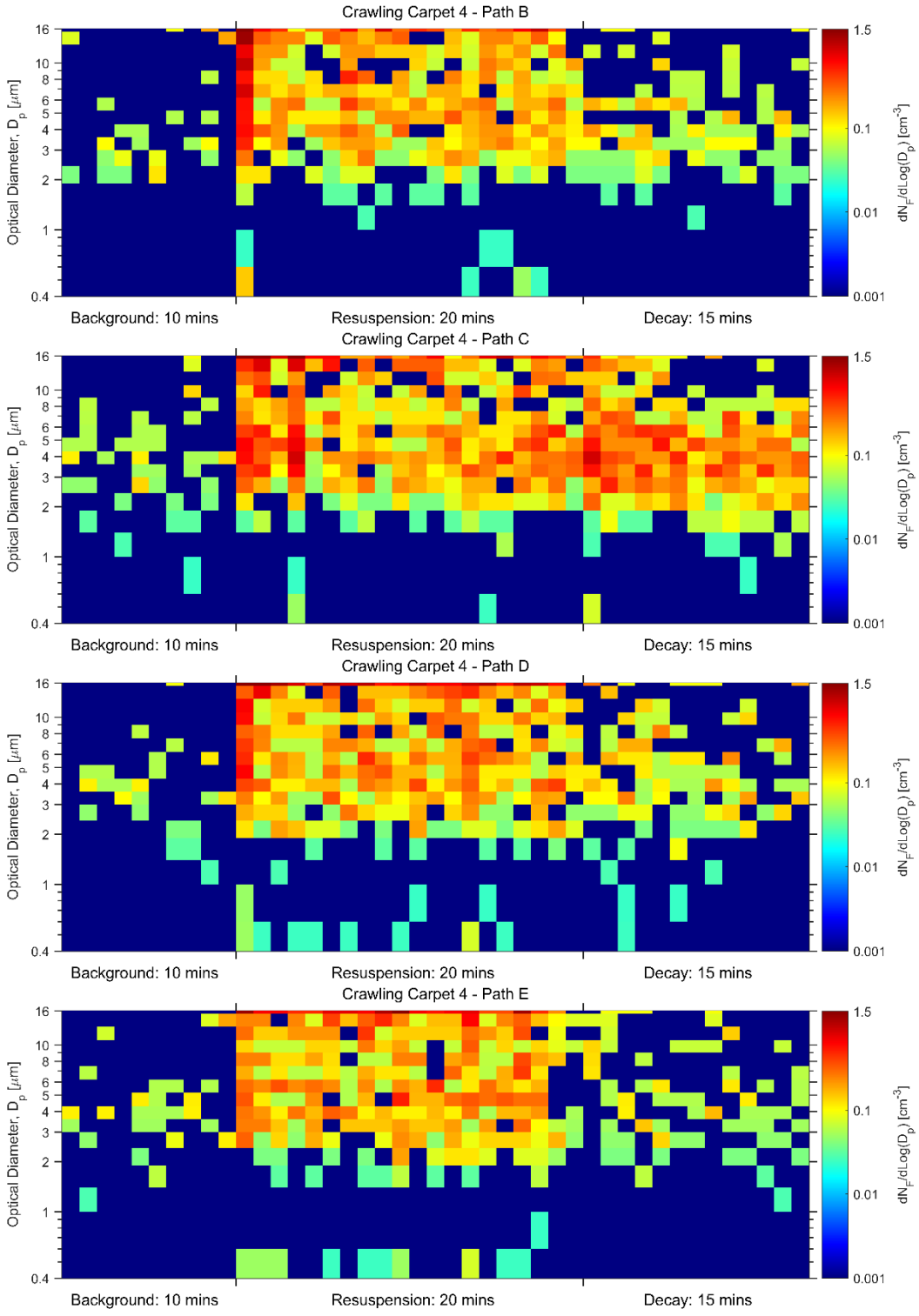
Crawling Carpet 4 - Path B
Optical Diameter, D_p [μm]
16
10
8
6
5
4
3
2
1
0.4
Background: 10 mins
Resuspension: 20 mins
Decay: 15 mins
1.5
0.1
0.01
0.001
$dN_F/dLog(D_p)$ [cm^{-3}]
Crawling Carpet 4 - Path C
Optical Diameter, D_p [μm]
Background: 10 mins
Resuspension: 20 mins
Decay: 15 mins
$dN_F/dLog(D_p)$ [cm^{-3}]
Crawling Carpet 4 - Path D
Optical Diameter, D_p [μm]
Background: 10 mins
Resuspension: 20 mins
Decay: 15 mins
$dN_F/dLog(D_p)$ [cm^{-3}]
Crawling Carpet 4 - Path E
Optical Diameter, D_p [μm]
Background: 10 mins
Resuspension: 20 mins
Decay: 15 mins
$dN_F/dLog(D_p)$ [cm^{-3}]

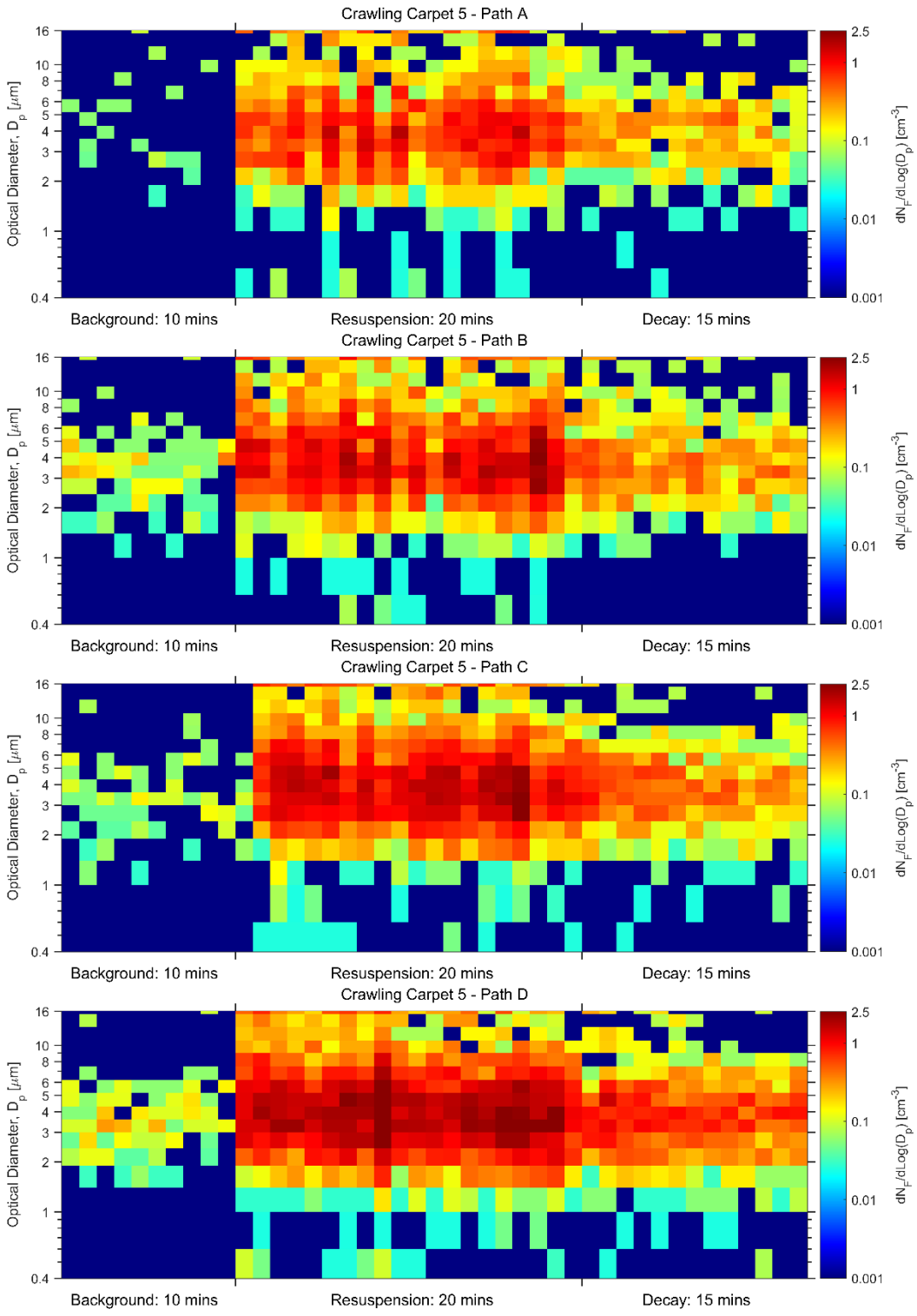
Crawling Carpet 5 - Path A
Optical Diameter, D_p [μm]
16
10
8
6
5
4
3
2
1
0.4
2.5
1
0.1
0.01
0.001
$dN_F/dLog(D_p)$ [cm^{-3}]
Background: 10 mins
Resuspension: 20 mins
Decay: 15 mins
Crawling Carpet 5 - Path B
Optical Diameter, D_p [μm]
$dN_F/dLog(D_p)$ [cm^{-3}]
Background: 10 mins
Resuspension: 20 mins
Decay: 15 mins
Crawling Carpet 5 - Path C
Optical Diameter, D_p [μm]
$dN_F/dLog(D_p)$ [cm^{-3}]
Background: 10 mins
Resuspension: 20 mins
Decay: 15 mins
Crawling Carpet 5 - Path D
Optical Diameter, D_p [μm]
$dN_F/dLog(D_p)$ [cm^{-3}]
Background: 10 mins
Resuspension: 20 mins
Decay: 15 mins

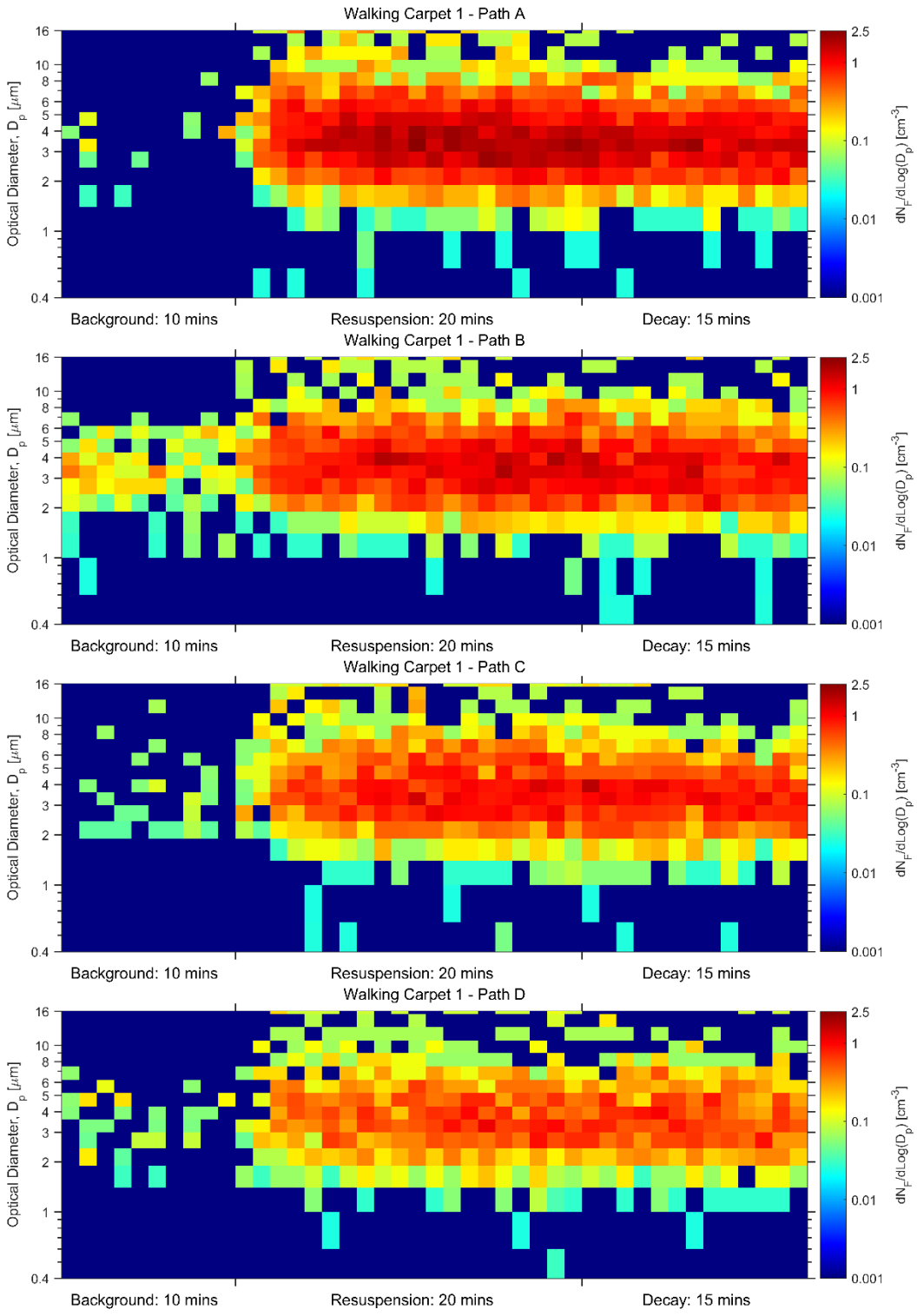
Walking Carpet 1 - Path A
Optical Diameter, D_p [μm]
16
10
8
6
5
4
3
2
1
0.4
2.5
1
0.1
0.01
0.001
$dN_F/dLog(D_p)$ [cm^{-3}]
Background: 10 mins
Resuspension: 20 mins
Decay: 15 mins
Walking Carpet 1 - Path B
Optical Diameter, D_p [μm]
$dN_F/dLog(D_p)$ [cm^{-3}]
Background: 10 mins
Resuspension: 20 mins
Decay: 15 mins
Walking Carpet 1 - Path C
Optical Diameter, D_p [μm]
$dN_F/dLog(D_p)$ [cm^{-3}]
Background: 10 mins
Resuspension: 20 mins
Decay: 15 mins
Walking Carpet 1 - Path D
Optical Diameter, D_p [μm]
$dN_F/dLog(D_p)$ [cm^{-3}]
Background: 10 mins
Resuspension: 20 mins
Decay: 15 mins

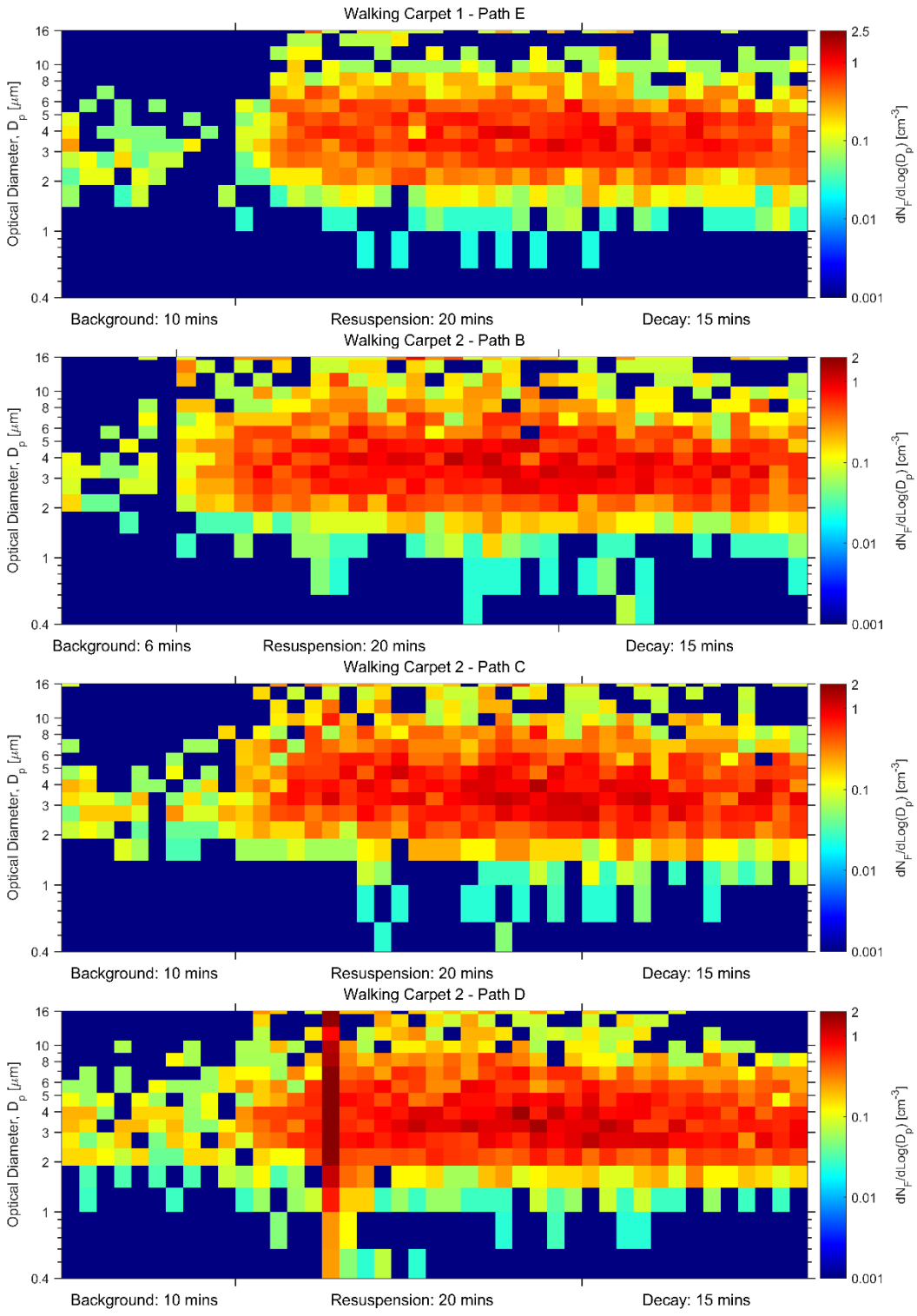
Walking Carpet 1 - Path E
Optical Diameter, D_p [μm]
16
10
8
6
5
4
3
2
1
0.4
2.5
1
0.1
0.01
0.001
dN_F/dLog(D_p) [cm^-3]
Background: 10 mins
Resuspension: 20 mins
Decay: 15 mins
Walking Carpet 2 - Path B
Optical Diameter, D_p [μm]
2
1
0.1
0.01
0.001
dN_F/dLog(D_p) [cm^-3]
Background: 6 mins
Resuspension: 20 mins
Decay: 15 mins
Walking Carpet 2 - Path C
Optical Diameter, D_p [μm]
2
1
0.1
0.01
0.001
dN_F/dLog(D_p) [cm^-3]
Background: 10 mins
Resuspension: 20 mins
Decay: 15 mins
Walking Carpet 2 - Path D
Optical Diameter, D_p [μm]
2
1
0.1
0.01
0.001
dN_F/dLog(D_p) [cm^-3]
Background: 10 mins
Resuspension: 20 mins
Decay: 15 mins

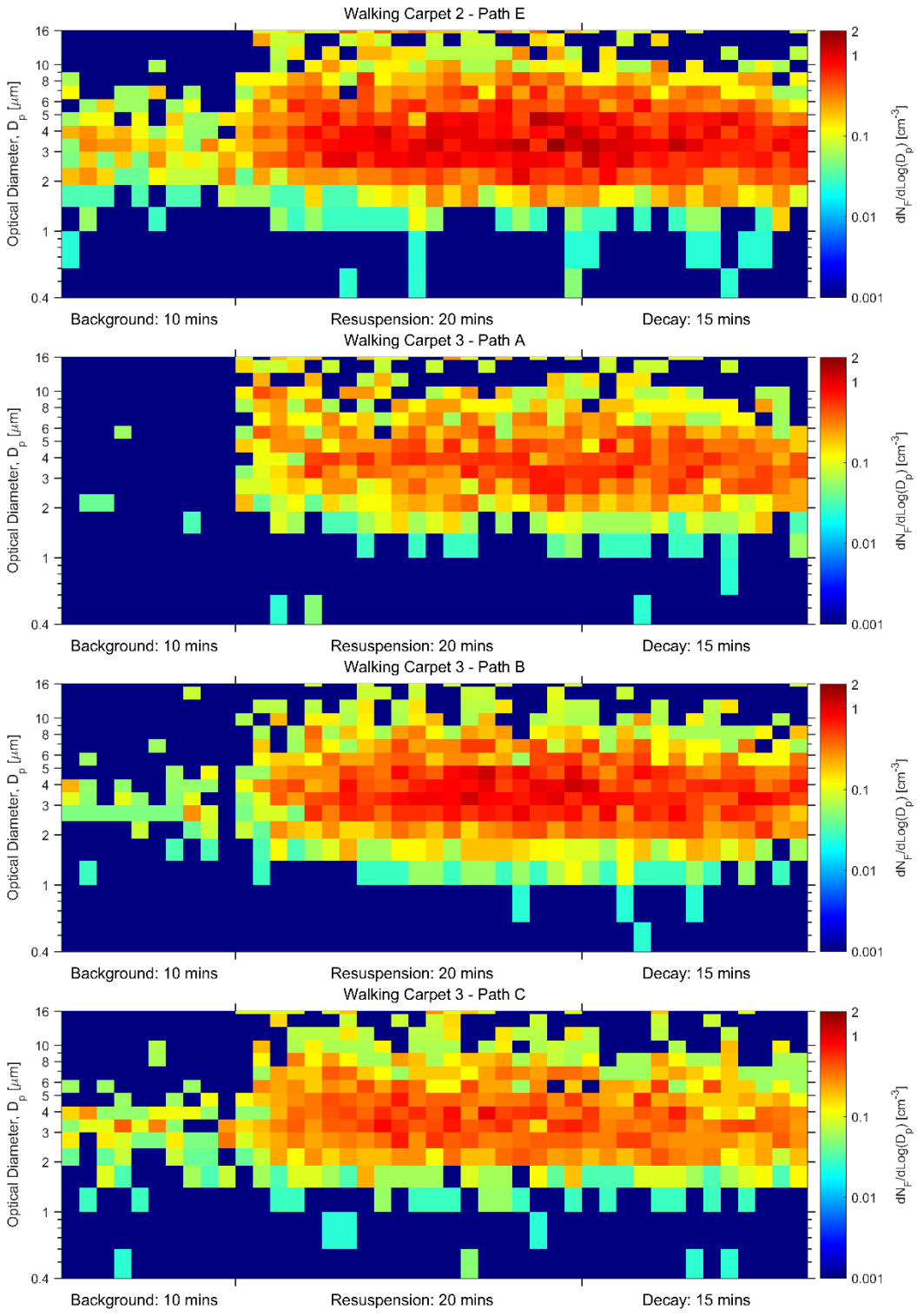
Walking Carpet 2 - Path E
Walking Carpet 3 - Path A
Walking Carpet 3 - Path B
Walking Carpet 3 - Path C
Optical Diameter, D_p [μm]
16
10
8
6
5
4
3
2
1
0.4
Background: 10 mins
Resuspension: 20 mins
Decay: 15 mins
$dN_F/dLog(D_p)$ [cm^{-3}]
2
1
0.1
0.01
0.001

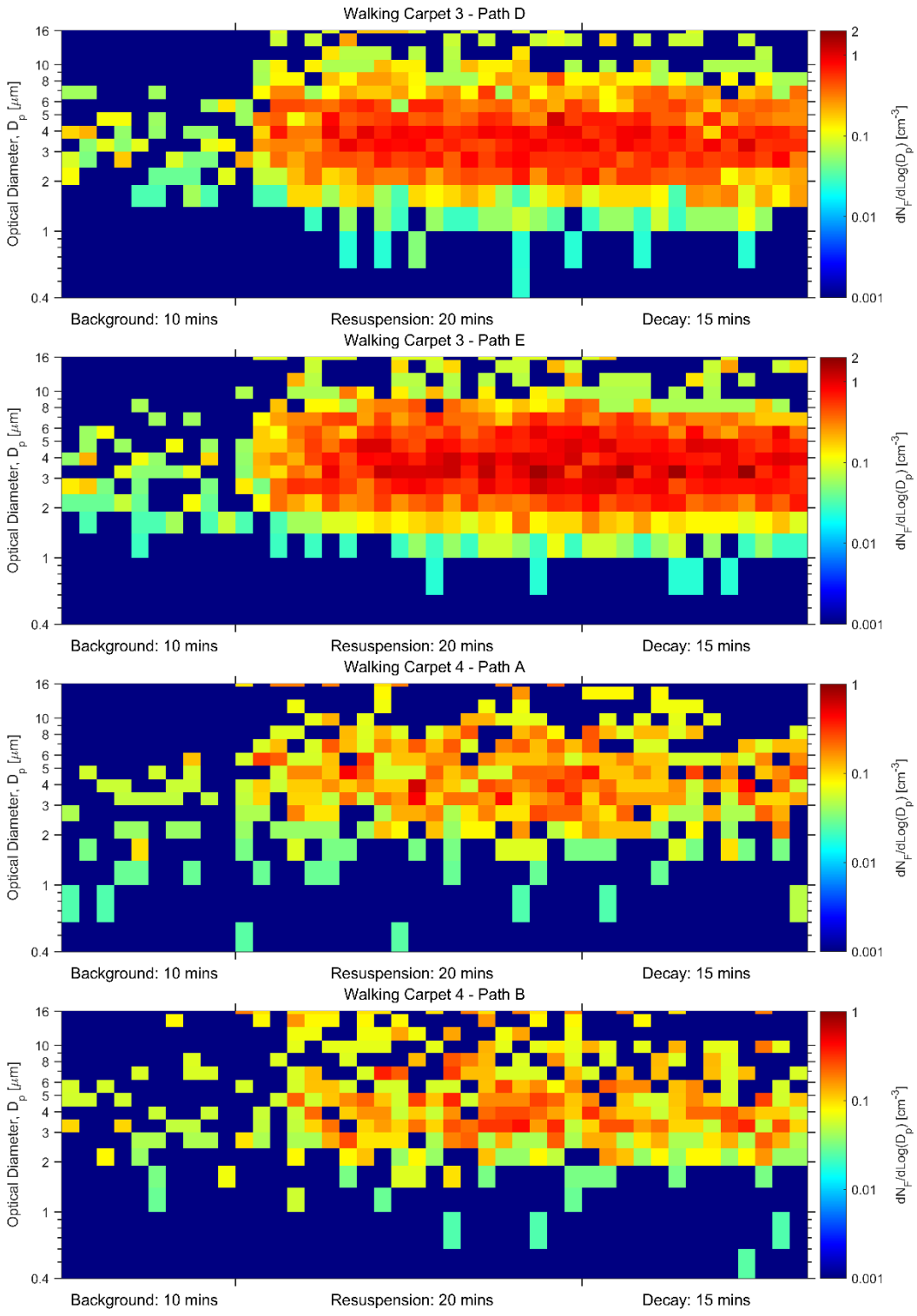
Walking Carpet 3 - Path D
Optical Diameter, D_p [μm]
16
10
8
6
5
4
3
2
1
0.4
Background: 10 mins
Resuspension: 20 mins
Decay: 15 mins
2
1
0.1
0.01
0.001
$dN_F/dLog(D_p)$ [cm^{-3}]
Walking Carpet 3 - Path E
Optical Diameter, D_p [μm]
16
10
8
6
5
4
3
2
1
0.4
Background: 10 mins
Resuspension: 20 mins
Decay: 15 mins
2
1
0.1
0.01
0.001
$dN_F/dLog(D_p)$ [cm^{-3}]
Walking Carpet 4 - Path A
Optical Diameter, D_p [μm]
16
10
8
6
5
4
3
2
1
0.4
Background: 10 mins
Resuspension: 20 mins
Decay: 15 mins
1
0.1
0.01
0.001
$dN_F/dLog(D_p)$ [cm^{-3}]
Walking Carpet 4 - Path B
Optical Diameter, D_p [μm]
16
10
8
6
5
4
3
2
1
0.4
Background: 10 mins
Resuspension: 20 mins
Decay: 15 mins
1
0.1
0.01
0.001
$dN_F/dLog(D_p)$ [cm^{-3}]

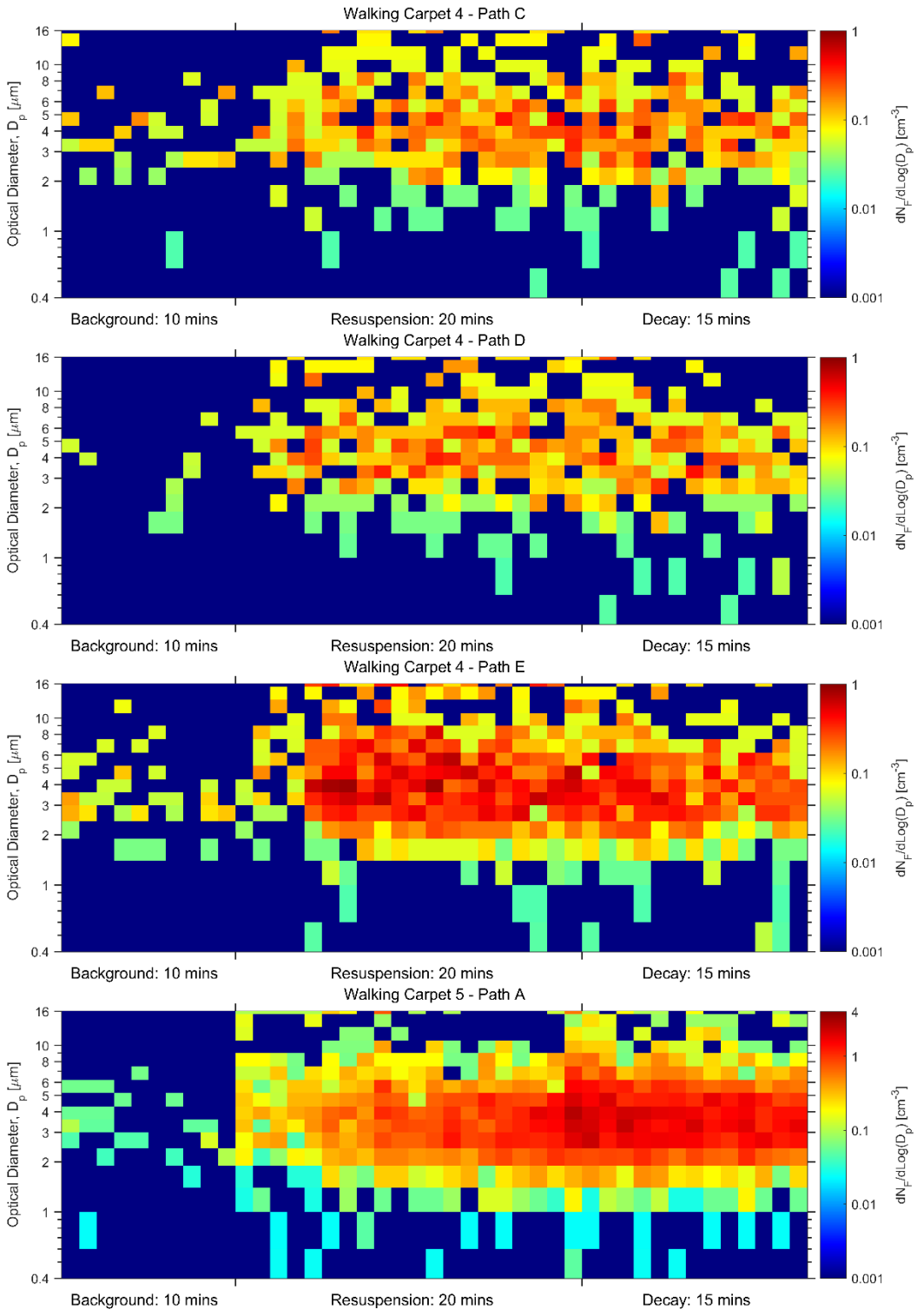
Walking Carpet 4 - Path C
Optical Diameter, D_p [μm]
16
10
8
6
5
4
3
2
1
0.4
Background: 10 mins
Resuspension: 20 mins
Decay: 15 mins
1
0.1
0.01
0.001
$dN_F/dLog(D_p)$ [cm^{-3}]
Walking Carpet 4 - Path D
Optical Diameter, D_p [μm]
Background: 10 mins
Resuspension: 20 mins
Decay: 15 mins
$dN_F/dLog(D_p)$ [cm^{-3}]
Walking Carpet 4 - Path E
Optical Diameter, D_p [μm]
Background: 10 mins
Resuspension: 20 mins
Decay: 15 mins
$dN_F/dLog(D_p)$ [cm^{-3}]
Walking Carpet 5 - Path A
Optical Diameter, D_p [μm]
Background: 10 mins
Resuspension: 20 mins
Decay: 15 mins
4
1
0.1
0.01
0.001
$dN_F/dLog(D_p)$ [cm^{-3}]

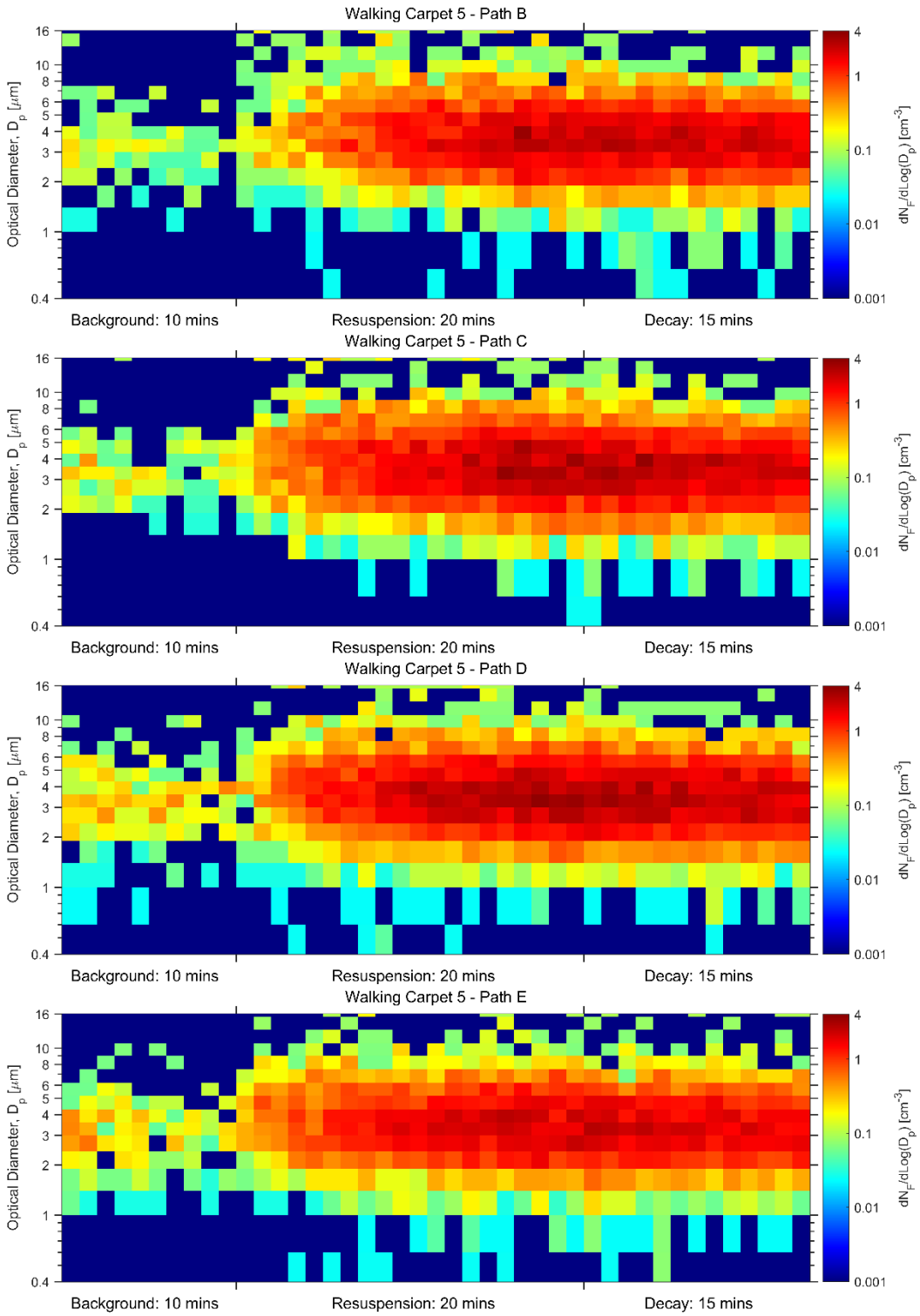

Figure S8. Time-series plots of FBAP number size distributions ($dN_F/dlogD_p$) for all fifty crawling (infant breathing zone) and walking (adult breathing zone) resuspension experiments.

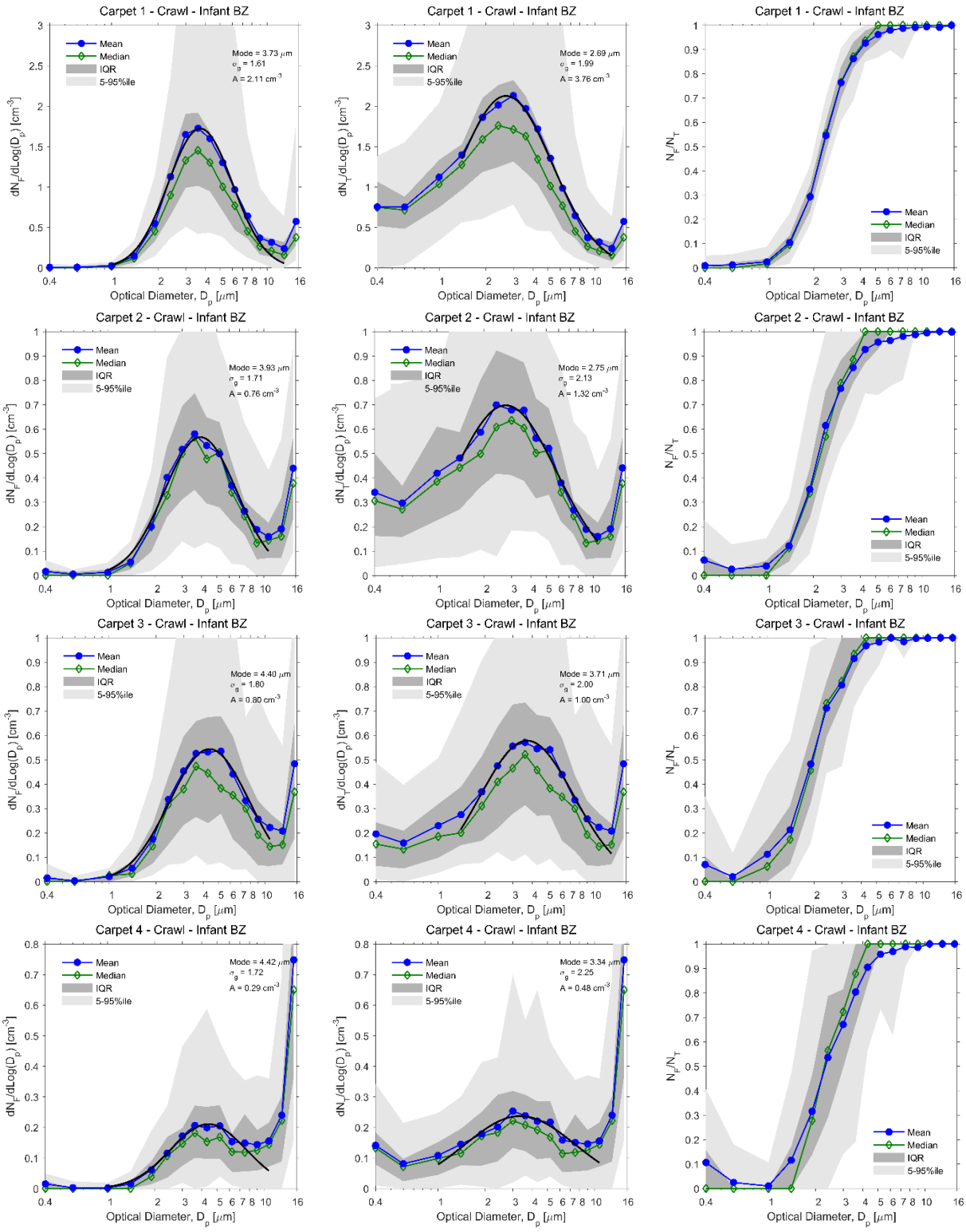
Carpet 1 - Crawl - Infant BZ
Mean
Median
IQR
5-95%ile
Mode = 3.73 μm
σg = 1.61
A = 2.11 cm-3
dNF/dLog(Dp) [cm-3]
Optical Diameter, Dp [μm]
Carpet 1 - Crawl - Infant BZ
Mean
Median
IQR
5-95%ile
Mode = 2.69 μm
σg = 1.99
A = 3.76 cm-3
dNT/dLog(Dp) [cm-3]
Optical Diameter, Dp [μm]
Carpet 1 - Crawl - Infant BZ
Mean
Median
IQR
5-95%ile
NF/NT
Optical Diameter, Dp [μm]
Carpet 2 - Crawl - Infant BZ
Mean
Median
IQR
5-95%ile
Mode = 3.93 μm
σg = 1.71
A = 0.76 cm-3
dNF/dLog(Dp) [cm-3]
Optical Diameter, Dp [μm]
Carpet 2 - Crawl - Infant BZ
Mean
Median
IQR
5-95%ile
Mode = 2.75 μm
σg = 2.13
A = 1.32 cm-3
dNT/dLog(Dp) [cm-3]
Optical Diameter, Dp [μm]
Carpet 2 - Crawl - Infant BZ
Mean
Median
IQR
5-95%ile
NF/NT
Optical Diameter, Dp [μm]
Carpet 3 - Crawl - Infant BZ
Mean
Median
IQR
5-95%ile
Mode = 4.40 μm
σg = 1.80
A = 0.80 cm-3
dNF/dLog(Dp) [cm-3]
Optical Diameter, Dp [μm]
Carpet 3 - Crawl - Infant BZ
Mean
Median
IQR
5-95%ile
Mode = 3.71 μm
σg = 2.00
A = 1.00 cm-3
dNT/dLog(Dp) [cm-3]
Optical Diameter, Dp [μm]
Carpet 3 - Crawl - Infant BZ
Mean
Median
IQR
5-95%ile
NF/NT
Optical Diameter, Dp [μm]
Carpet 4 - Crawl - Infant BZ
Mean
Median
IQR
5-95%ile
Mode = 4.42 μm
σg = 1.72
A = 0.29 cm-3
dNF/dLog(Dp) [cm-3]
Optical Diameter, Dp [μm]
Carpet 4 - Crawl - Infant BZ
Mean
Median
IQR
5-95%ile
Mode = 3.34 μm
σg = 2.25
A = 0.48 cm-3
dNT/dLog(Dp) [cm-3]
Optical Diameter, Dp [μm]
Carpet 4 - Crawl - Infant BZ
Mean
Median
IQR
5-95%ile
NF/NT
Optical Diameter, Dp [μm]

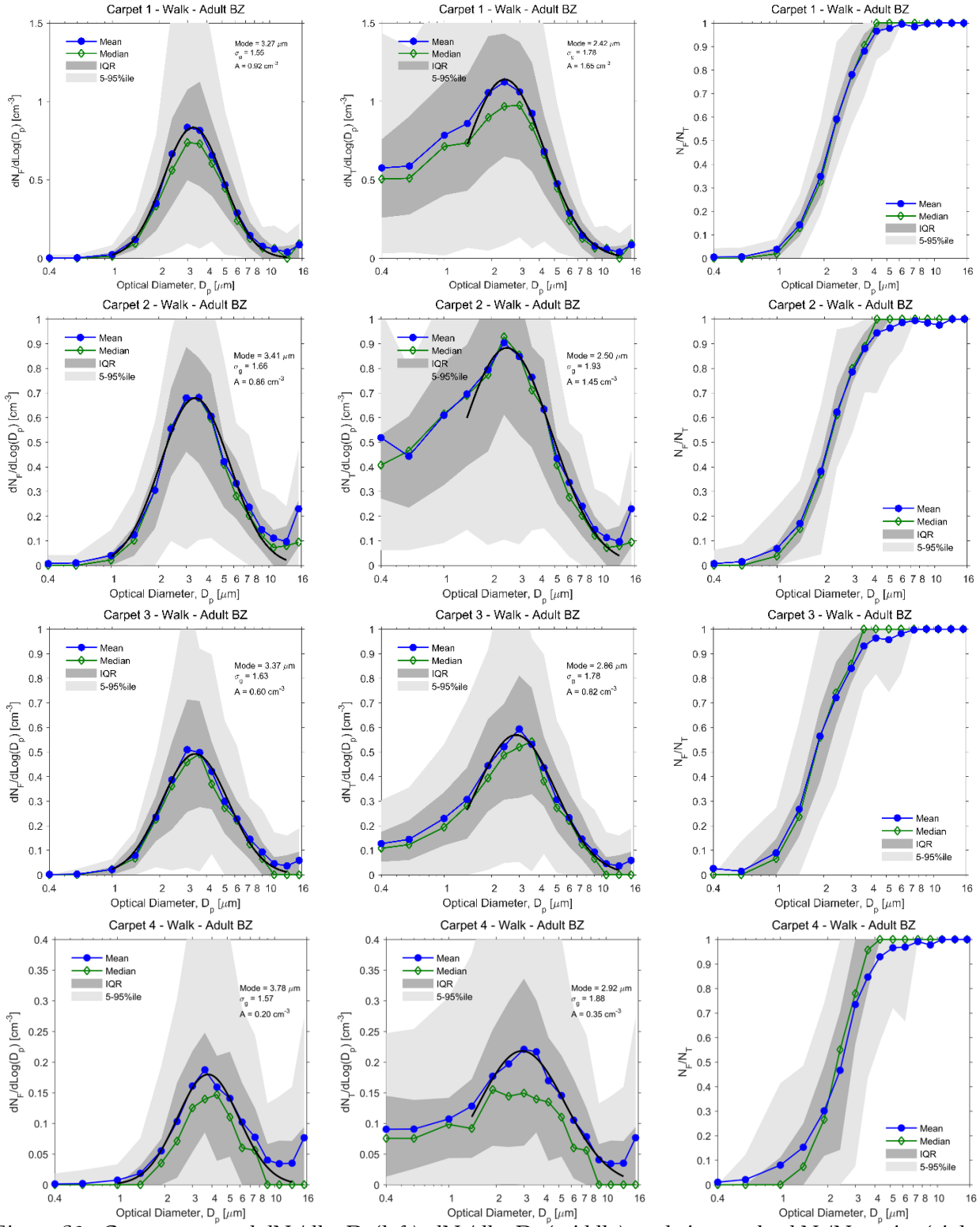

Figure S9. Carpet-averaged $dN_F/dlogD_p$ (left), $dN_T/dlogD_p$ (middle), and size-resolved N_F/N_T ratios (right) measured during the crawling and walking periods on carpets 1-4 (carpet 5 presented in the main body of the text). Blue curves represent mean values, green curves represent median values, dark gray regions represent the interquartile range (IQR), and light gray regions represent the 5-95th percentile range among five crawling or walking paths on the same carpet (100 minutes in total). Black curves show the lognormal fitting of the dominant peaks. The mode, geometric standard deviation (σ_g), and amplitude (A) are presented.

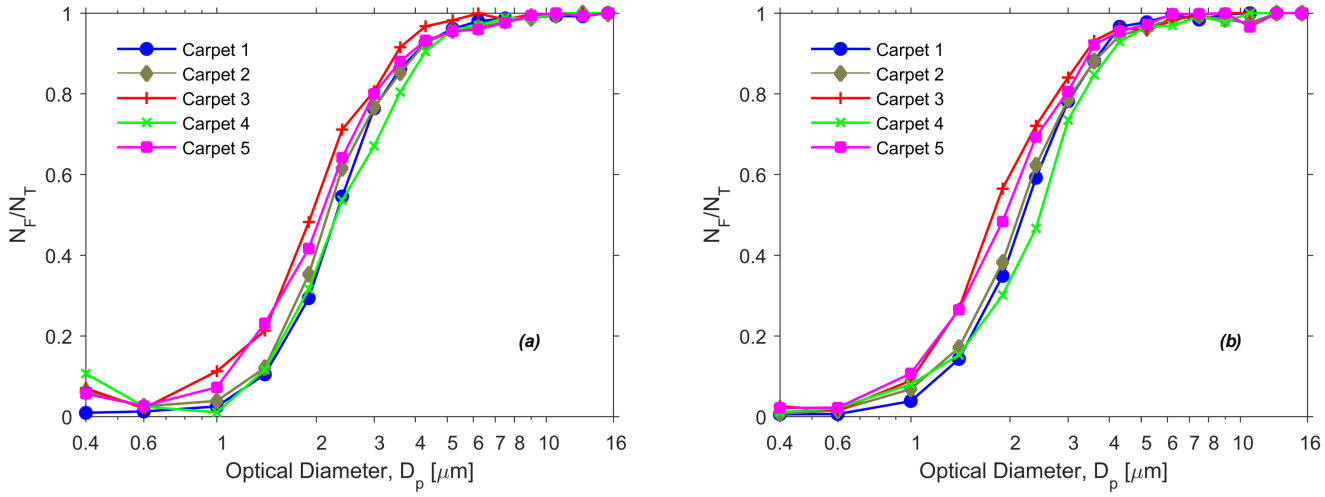

Figure S10. Carpet-averaged size-resolved N_F/N_T ratios measured during resuspension periods on five carpets for both crawling (a.) and walking (b.) experiments.

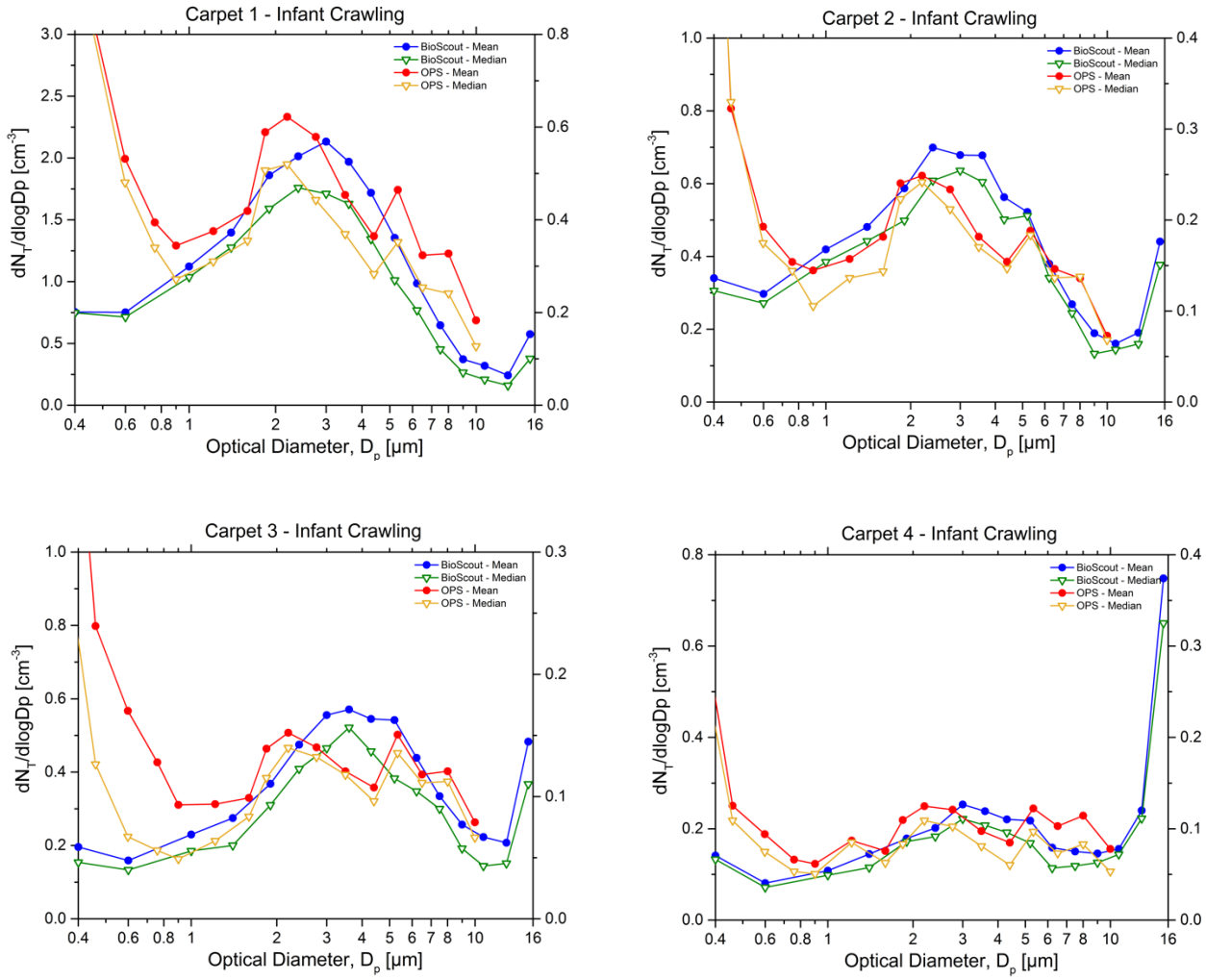

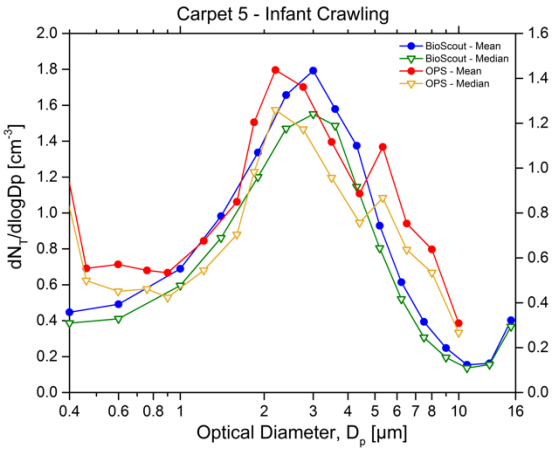
Carpet 5 - Infant Crawling
BioScout - Mean
BioScout - Median
OPS - Mean
OPS - Median
dN_T/dlogDp [cm^-3]
Optical Diameter, D_p [µm]

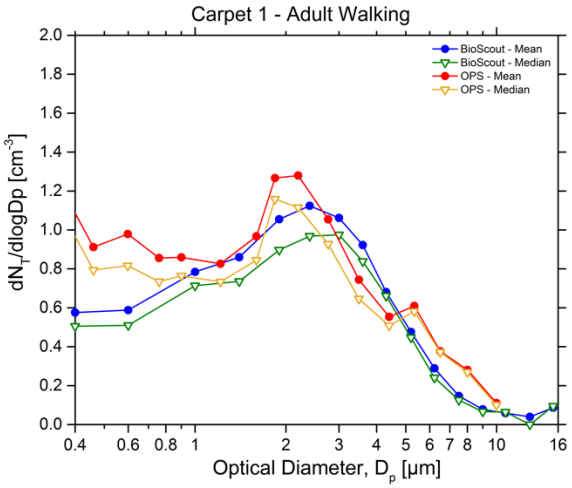
Carpet 1 - Adult Walking
BioScout - Mean
BioScout - Median
OPS - Mean
OPS - Median
dN_T/dlogDp [cm^-3]
Optical Diameter, D_p [µm]

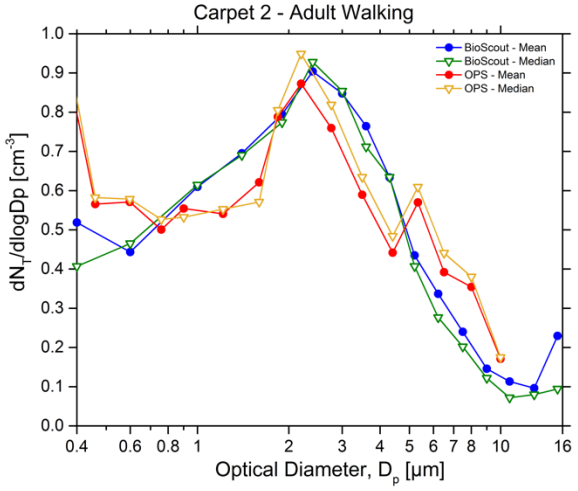
Carpet 2 - Adult Walking
BioScout - Mean
BioScout - Median
OPS - Mean
OPS - Median
dN_T/dlogDp [cm^-3]
Optical Diameter, D_p [µm]

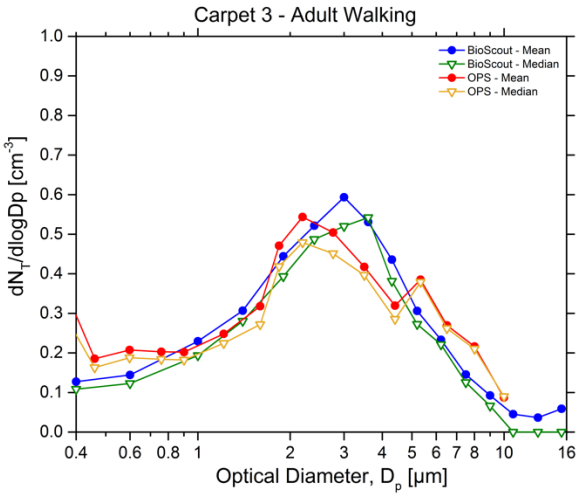
Carpet 3 - Adult Walking
BioScout - Mean
BioScout - Median
OPS - Mean
OPS - Median
dN_T/dlogDp [cm^-3]
Optical Diameter, D_p [µm]

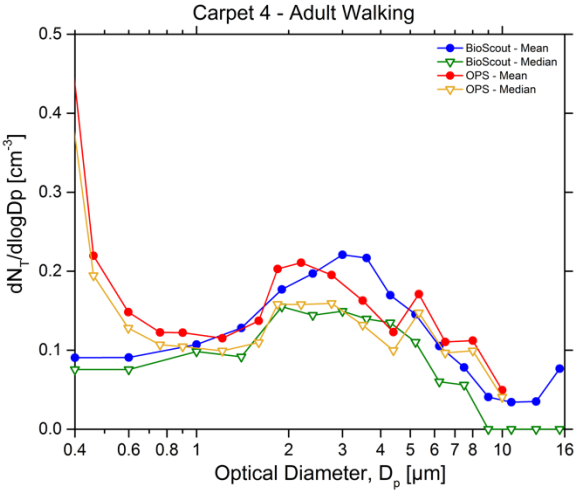
Carpet 4 - Adult Walking
BioScout - Mean
BioScout - Median
OPS - Mean
OPS - Median
dN_T/dlogDp [cm^-3]
Optical Diameter, D_p [µm]

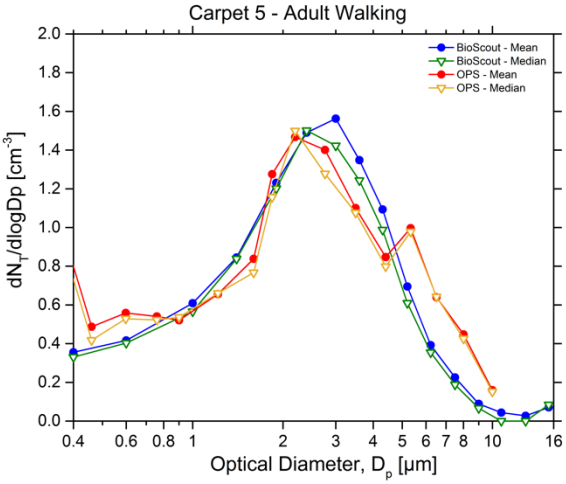

Figure S11. Median and mean total particle size distributions as measured by the BioScout and OPS during the resuspension periods in the crawling and walking experiments on all five carpets. The size distributions measured by the OPS in the crawling experiments were re-scaled on a secondary y-axis.

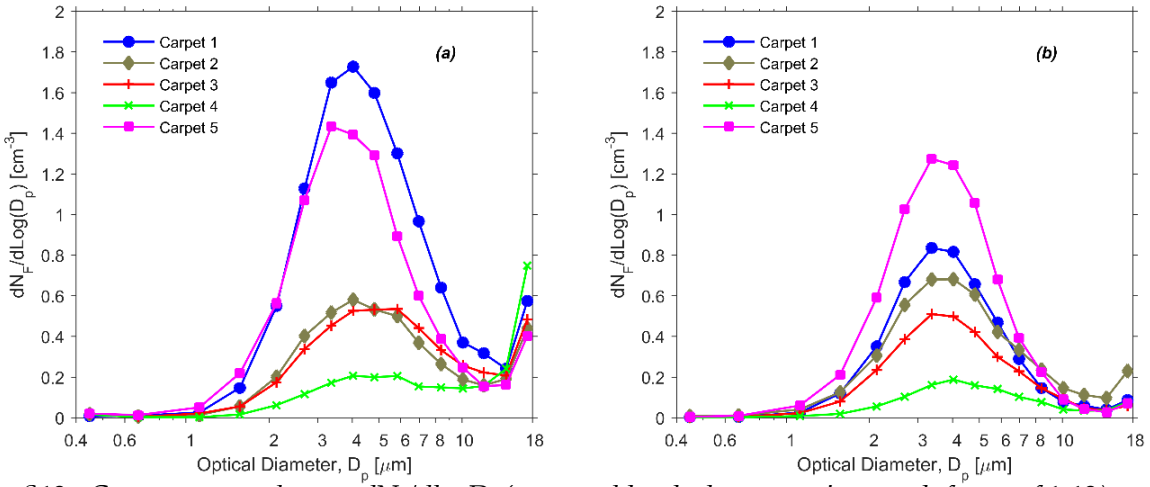

Figure S12. Carpet-averaged mean $dN_F/dlogD_p$ (corrected by the hygroscopic growth factor of 1.12) measured during the resuspension periods on five carpets for both crawling (a.) and walking (b.) experiments. Note: the size distributions are slightly shifted to the right, with an upper-limit of 18 µm, compared to Figure 3, due to hygroscopic particle growth.

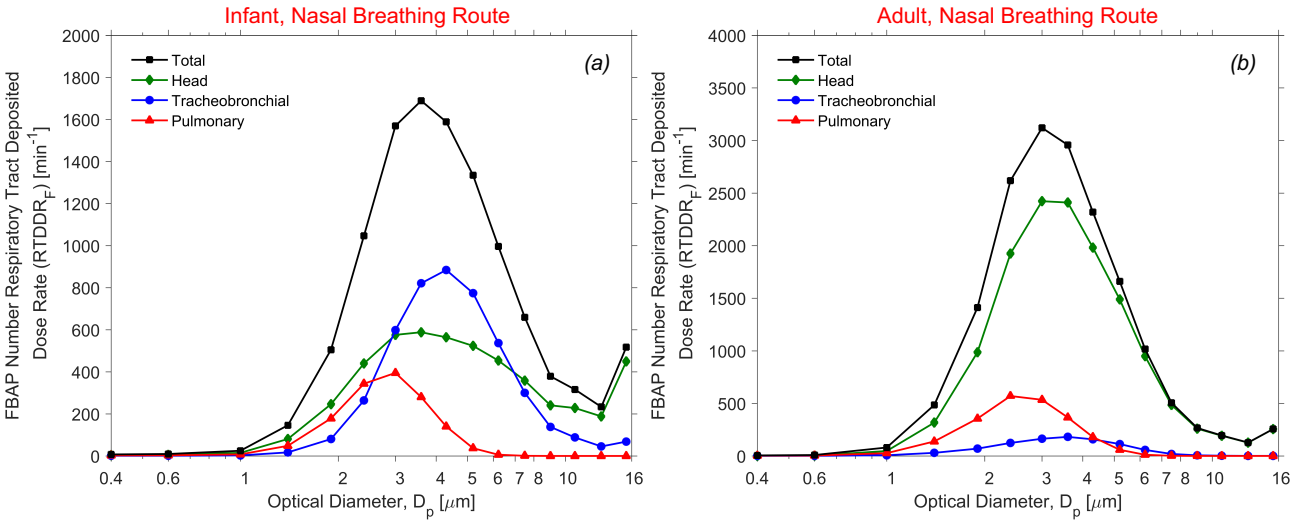

*Figure S13. Total and regional size-resolved FBAP number respiratory tract deposited dose rates (RTDDR$_F$s) (per minute crawling or walking) on carpet 1, for (a.) infant crawling, nasal breathing route, (b.) adult walking, nasal breathing route. Note: the hygroscopic growth factor was **not** applied.*

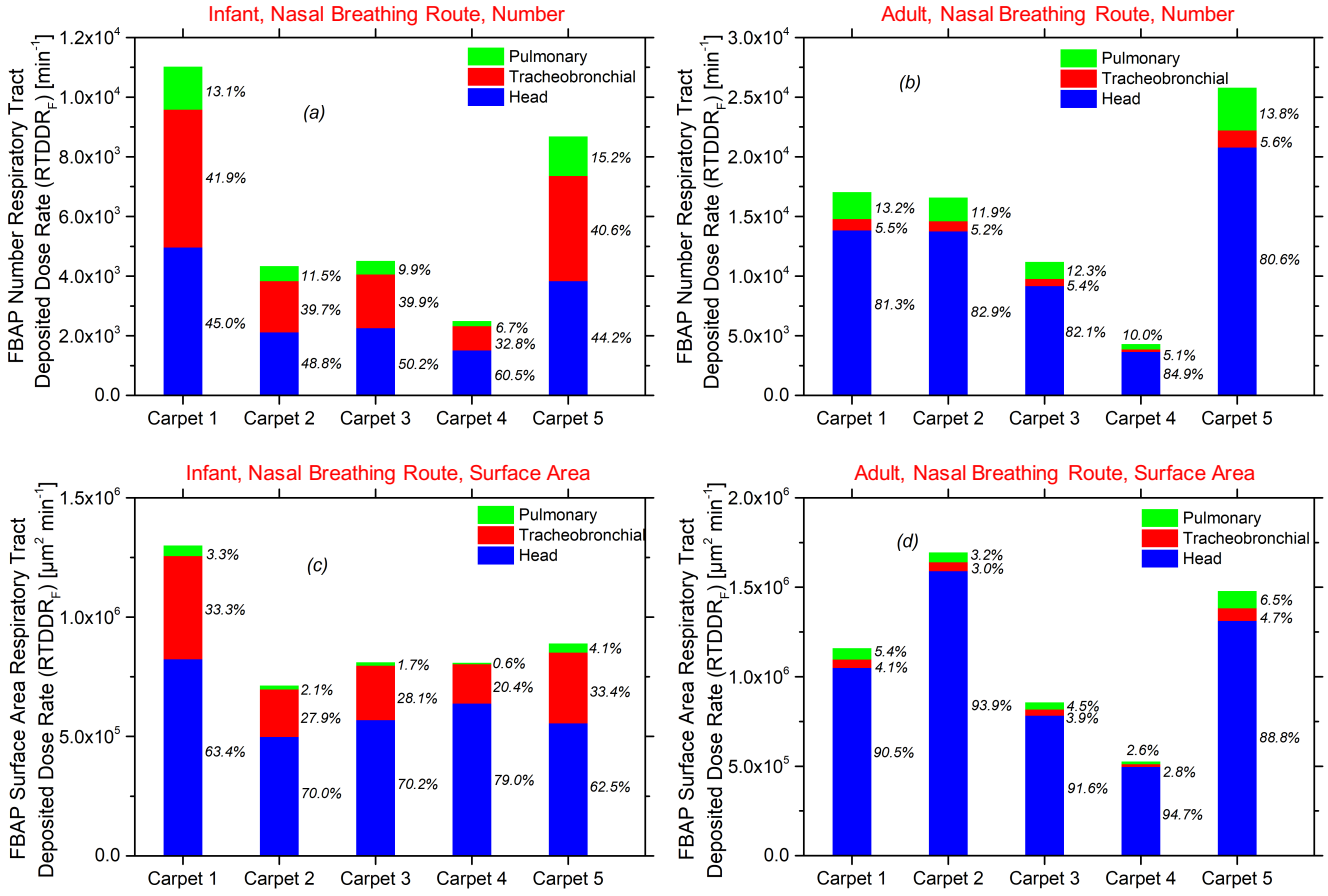

*Figure S14. Total and regional size-integrated (0.4-15.4 μm) FBAP respiratory tract deposited dose rates (RTDDR$_F$s) (per minute crawling or walking) for each of the five carpets (a.) infant, nasal breathing route, number, (b.) adult, nasal breathing route, number, (c.) infant, nasal breathing route, surface area, and (d.) adult, nasal breathing route, surface area. The fractional dose in each region, expressed as a percentage, is shown to the right of each bar. Note: the hygroscopic growth factor was **not** applied.*

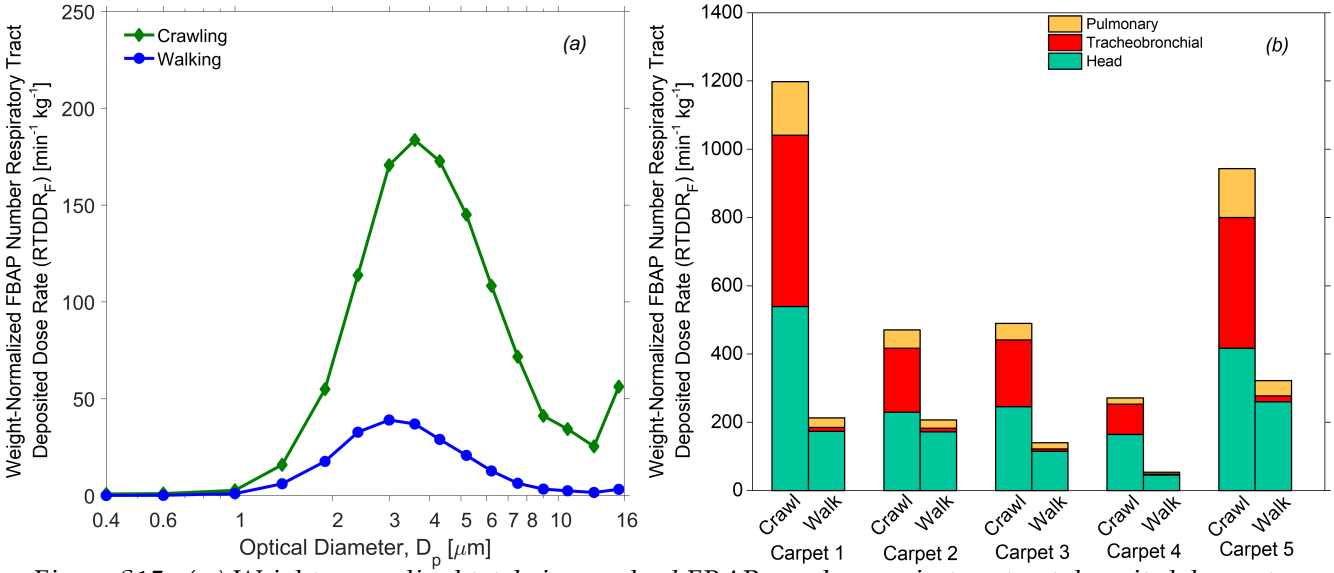

*Figure S15. (a.) Weight-normalized total size-resolved FBAP number respiratory tract deposited dose rates (RTDDR$_F$s) for infant crawling and adult walking on carpet 1 (both nasal breathing route) and (b.) weight-normalized regional size-integrated (0.4-15.4 μm) FBAP number RTDDR$_F$s for infant crawling and adult walking on each of the five carpets (both nasal breathing route). Note in (b.), a log-scale is used for the y-axis to improve visualization of the difference in weight-normalized doses between an infant and adult. Note: the hygroscopic growth factor was **not** applied.*

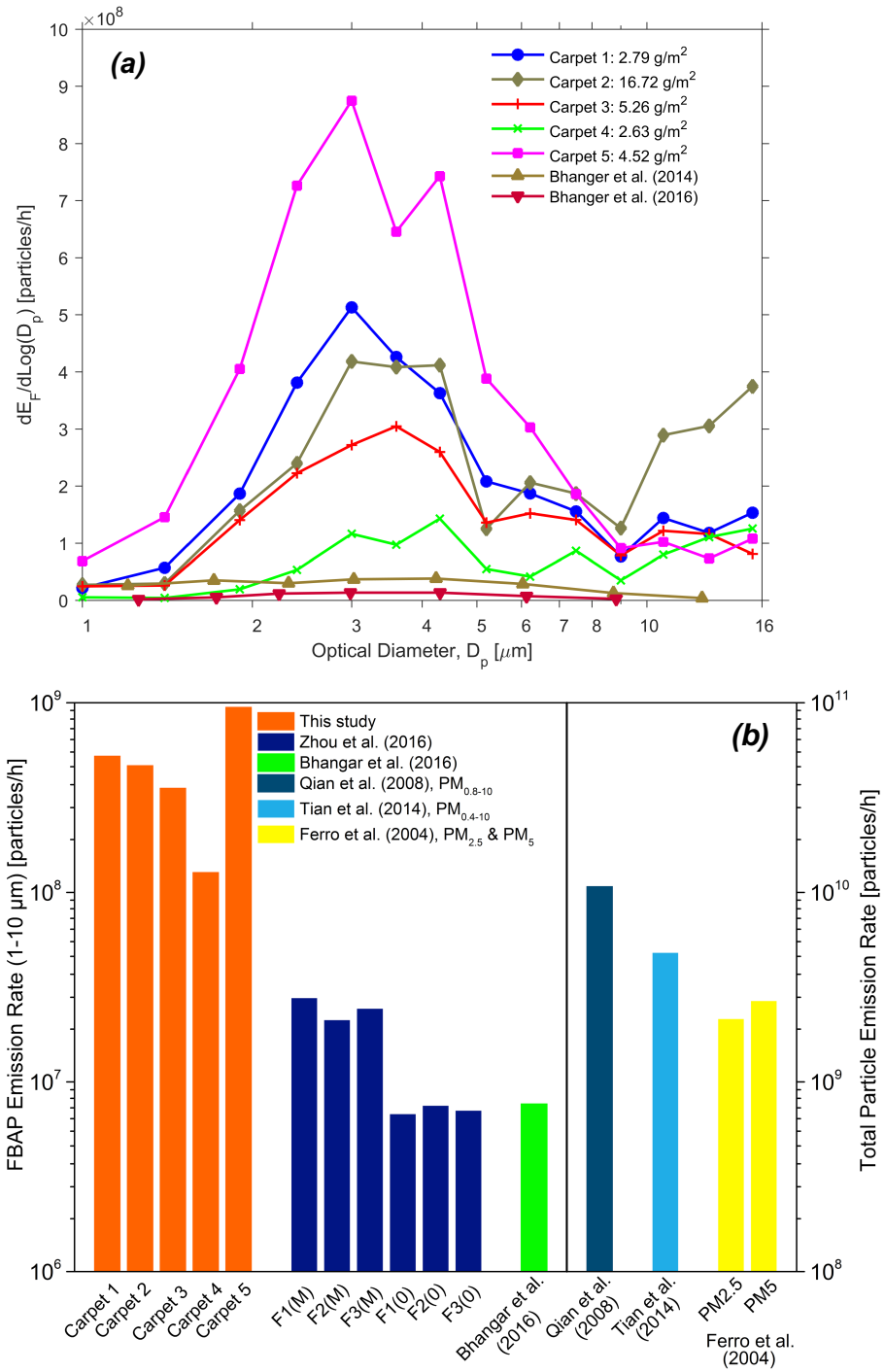

Figure S16. (a.) Size-resolved log-normalized emission rates of resuspended FBAPs during the adult walking experiments on each of the five carpets, per-person FBAP emission rates during the transition periods in a university classroom (Bhangar et al. (3)), and per-person FBAP emission rates for walking on carpet in a controlled chamber (Bhangar et al. (4)), assuming that the CO_2 emission rate during walking is 38 g/min (Bhangar et al. (4)), and (b.) carpet-averaged size-integrated (1-10 μm) emission rates of resuspended FBAPs during the adult walking experiments on each of the five carpets (this study), size-integrated FBAP emission rates of three volunteers (F1, F2, F3) measured during walking on vinyl flooring in a chamber (Zhou et al. (87)) ('M' and '0' represent with and without the application of moisturizer, respectively), size-integrated FBAP emission rates for walking on carpet in a controlled chamber (Bhangar et al. (4)), and size-integrated total particle emission rates for walking-induced resuspension from Qian et al. (51), Tian et al. (74), and Ferro et al. (20), the latter three of which are presented on a re-scaled secondary y-axis. Note: the particle size reported in this study, Zhou et al. (87), Qian et al. (51), and Tian et al. (74) is an optical diameter, whereas the particle size measured by Bhangar et al. (3, 4) and Ferro et al. (20) is an aerodynamic diameter.

References

(1) Adams, R. I.; Bhangar, S.; Pasut, W.; Arens, E. A.; Taylor, J. W.; Lindow, S. E.; Nazaroff, W. W.; Bruns, T. D. Chamber bioaerosol study: Outdoor air and human occupants as sources of indoor airborne microbes. *PLoS One* **2015**, *10* (7), 1–18.

(2) Balaev, A. E.; Dvoretski, K. N.; Doubrovski, V. A. Determination of refractive index of rod-shaped bacteria from spectral extinction measurements. In *Proceedings of SPIE*; **2003**; Vol. 5068, pp 375–380.

(3) Bhangar, S.; Huffman, J. A.; Nazaroff, W. W. Size-resolved fluorescent biological aerosol particle concentrations and occupant emissions in a university classroom. *Indoor Air*. **2014**, pp 604–617.

(4) Bhangar, S.; Adams, R. I.; Pasut, W.; Huffman, J. A.; Arens, E. A.; Taylor, J. W.; Bruns, T. D.; Nazaroff, W. W. Chamber bioaerosol study: Human emissions of size-resolved fluorescent biological aerosol particles. *Indoor Air* **2016**, *26* (2), 193–206.

(5) Bisgaard, H.; Hermansen, M. N.; Buchvald, F.; Loland, L.; Halkjaer, L. B.; Bønnelykke, K.; Brasholt, M.; Heltberg, A.; Vissing, N. H.; Thorsen, S. V. Childhood asthma after bacterial colonization of the airway in neonates. *N. Engl. J. Med.* **2007**, *357* (15), 1487–1495.

(6) Bliznakova, I.; Borisova, E.; Avramov, L. Laser-and light-induced autofluorescence spectroscopy of human skin in dependence on excitation wavelengths. *ACTA Phys. Pol. Ser. A* **2007**, *112* (5), 1131.

(7) Boor, B. E.; Siegel, J. A.; Novoselac, A. Monolayer and multilayer particle deposits on hard surfaces: literature review and implications for particle resuspension in the indoor environment. *Aerosol Sci. Technol.* **2013**, *47* (8), 831–847.

(8) Boor, B. E.; Spilak, M. P.; Corsi, R. L.; Novoselac, A. Characterizing particle resuspension from mattresses: Chamber study. *Indoor Air* **2015**, *25* (4), 441–456.

(9) Calderón, M. A.; Linneberg, A.; Kleine-Tebbe, J.; De Blay, F.; Hernandez Fernandez De Rojas, D.; Virchow, J. C.; Demoly, P. Respiratory allergy caused by house dust mites: What do we really know? *J. Allergy Clin. Immunol.* **2015**, *136* (1), 38–48.

(10) Dannemiller, K. C.; Gent, J. F.; Leaderer, B. P.; Peccia, J. Influence of housing characteristics on bacterial and fungal communities in homes of asthmatic children. *Indoor Air* **2016**, *26* (2), 179–192.

(11) Dannemiller, K. C.; Mendell, M. J.; Macher, J. M.; Kumagai, K.; Bradman, A.; Holland, N.; Harley, K.; Eskenazi, B.; Peccia, J. Next‐generation DNA sequencing reveals that low fungal diversity in house dust is associated with childhood asthma development. *Indoor Air* **2014**, *24* (3), 236–247.

(12) Davies, R. R.; Noble, W. C. Dispersal of bacteria on desquamated skin. *Lancet* **1962**, *280* (7269), 1295–1297.

(13) Davies, J. M.; Beggs, P. J.; Medek, D. E.; Newnham, R. M.; Erbas, B.; Thibaudon, M.; Katelaris, C. H.; Haberle, S. G.; Newbigin, E. J.; Huete, A. R. Trans-disciplinary research in synthesis of grass pollen aerobiology and its importance for respiratory health in Australasia. *Sci. Total Environ.* **2015**, *534*, 85–96.

(14) Denning, D. W.; O'Driscoll, B. R.; Hogaboam, C. M.; Bowyer, P.; Niven, R. M. The link between fungi and severe asthma: A summary of the evidence. *Eur. Respir. J.* **2006**, *27* (3), 615–626.

(15) Després, V. R.; Alex Huffman, J.; Burrows, S. M.; Hoose, C.; Safatov, A. S.; Buryak, G.; Fröhlich-Nowoisky, J.; Elbert, W.; Andreae, M. O.; Pöschl, U.; et al. Primary biological aerosol particles in the atmosphere: A review. *Tellus, Ser. B Chem. Phys. Meteorol.* **2012**, *64* (1).

(16) Ebert, M.; Weinbruch, S.; Rausch, A.; Gorzawski, G.; Helas, G.; Hoffmann, P.; Wex, H. Complex refractive index of aerosols during LACE 98# x2010; as derived from the analysis of individual particles. *J. Geophys. Res. Atmos.* **2002**, *107* (D21).

(17) Ege, M. J.; Mayer, M.; Normand, A.-C.; Genuneit, J.; Cookson, W. O. C. M.; Braun-Fahrländer, C.; Heederik, D.; Piarroux, R.; von Mutius, E. Exposure to environmental microorganisms and childhood asthma. *N. Engl. J. Med.* **2011**, *364* (8), 701–709.

(18) Ege, M. J.; Mayer, M.; Schwaiger, K.; Mattes, J.; Pershagen, G.; Van Hage, M.; Scheynius, A.; Bauer, J.; Von Mutius, E. Environmental bacteria and childhood asthma. *Allergy Eur. J. Allergy Clin. Immunol.* **2012**, *67* (12), 1565–1571.

(19) Fahlbusch, B.; Hornung, D.; Ja, L. Quantification of group 5 grass pollen allergens in house dust. *Clin. Exp. Allergy* **2000**, *30*, 1645–1652.

(20) Ferro, A. R.; Kopperud, R. J.; Hildemann, L. M. Source strengths for indoor human activities that resuspend particulate matter. *Environ. Sci. Technol.* **2004**, *38* (6), 1759–1764.

(21) Fröhlich-Nowoisky, J.; Burrows, S. M.; Xie, Z.; Engling, G.; Solomon, P. A.; Fraser, M. P.; Mayol-Bracero, O. L.; Artaxo, P.; Begerow, D.; Conrad, R. Biogeography in the air: fungal diversity over land and oceans. *Biogeosciences* **2012**, *9* (3), 1125.

(22) Gomes, C.; Freihaut, J.; Bahnfleth, W. Resuspension of allergen-containing particles under mechanical and aerodynamic disturbances from human walking. *Atmos. Environ.* **2007**, *41* (25), 5257–5270.

(23) Grinshpun, S.; Willeke, K.; Kalatoor, S. A general equation for aerosol aspiration by thin-walled sampling probes in calm and moving air. *Atmos. Environ. Part A. Gen. Top.* **1993**, *27* (9), 1459–1470.

(24) Hilty, M.; Burke, C.; Pedro, H.; Cardenas, P.; Bush, A.; Bossley, C.; Davies, J.; Ervine, A.; Poulter, L.; Pachter, L. Disordered microbial communities in asthmatic airways. *PLoS One* **2010**, *5* (1), e8578.
(25) Hinds, W. *Aerosol technology: properties, behavior, and measurement of airborne particles*; 2001; Vol. 2.
(26) Man, W. H.; de Steenhuijsen Piters, W. A. A.; Bogaert, D. The microbiota of the respiratory tract: gatekeeper to respiratory health. *Nat. Rev. Microbiol.* **2017**.
(27) Hofmann, W.; Martonen, T. B.; Graham, R. C. Predicted Deposition of Nonhygroscopic Aerosols in the Human Lung as a Function of Subject Age. *J. Aerosol Med.* **1989**, *2* (1), 49–68.
(28) Hospodsky, D.; Qian, J.; Nazaroff, W. W.; Yamamoto, N.; Bibby, K.; Rismani-Yazdi, H.; Peccia, J. Human occupancy as a source of indoor airborne bacteria. *PLoS One* **2012**, *7* (4).
(29) Hospodsky, D.; Yamamoto, N.; Peccia, J. Accuracy, precision, and method detection limits of quantitative PCR for airborne bacteria and fungi. *Appl. Environ. Microbiol.* **2010**, *76* (21), 7004–7012.
(30) Hospodsky, D.; Yamamoto, N.; Nazaroff, W. W.; Miller, D.; Gorthala, S.; Peccia, J. Characterizing airborne fungal and bacterial concentrations and emission rates in six occupied children's classrooms. *Indoor Air* **2015**, *25* (6), 641–652.
(31) Huffman, J. A.; Santarpia, J. Microbiology of Aerosols: Online Techniques for Quantification and Characterization of Biological Aerosols. **2017**, No. 6, 83.
(32) Hunt, A.; Johnson, D. L.; Griffith, D. A. Mass transfer of soil indoors by track-in on footwear. *Sci. Total Environ.* **2006**, *370* (2), 360–371.
(33) Hussein, T.; Löndahl, J.; Paasonen, P.; Koivisto, A. J.; Petäjä, T.; Hämeri, K.; Kulmala, M. Modeling regional deposited dose of submicron aerosol particles. *Sci. Total Environ.* **2013**, *458*, 140–149.
(34) Hyytiäinen, H.; Jayaprakash, B.; Kirjavainen, P.; Saari, S.; Holopainen, R.; Keskinen, J.; Hämeri, K.; Hyvärinen, A.; Boor, B. E.; Täubel, M. Crawling-Induced floor dust resuspension affects the microbiota of the infant breathing zone. *Microbiome*, In Press.
(35) Jamieson, K. S.; ApSimon, H. M.; Jamieson, S. S.; Bell, J. N. B.; Yost, M. G. The effects of electric fields on charged molecules and particles in individual microenvironments. *Atmos. Environ.* **2007**, *41* (25), 5224–5235.
(36) Lacks, D. J.; Mohan Sankaran, R. Contact electrification of insulating materials. *J. Phys. D. Appl. Phys.* **2011**, *44* (45), 453001.
(37) Lawson, J. A.; Dosman, J. A.; Rennie, D. C.; Beach, J. R.; Newman, S. C.; Crowe, T.; Senthilselvan, A. Endotoxin as a determinant of asthma and wheeze among rural dwelling children and adolescents: A case–control study. *BMC Pulm. Med.* **2012**, *12* (1), 56.
(38) Löndahl, J.; Massling, A.; Pagels, J.; Swietlicki, E.; Vaclavik, E.; Loft, S. Size-resolved respiratory-tract deposition of fine and ultrafine hydrophobic and hygroscopic aerosol particles during rest and exercise. *Inhal. Toxicol.* **2007**, *19* (2), 109–116.
(39) Lynch, S. V.; Wood, R. A.; Boushey, H.; Bacharier, L. B.; Bloomberg, G. R.; Kattan, M.; O'Connor, G. T.; Sandel, M. T.; Calatroni, A.; Matsui, E.; et al. Effects of early-life exposure to allergens and bacteria on recurrent wheeze and atopy in urban children. *J. Allergy Clin. Immunol.* **2014**, *134* (3).
(40) Mackintosh, C. A.; Lidwell, O. M.; Towers, A. G.; Marples, R. R. The dimensions of skin fragments dispersed into the air during activity. *Epidemiol. Infect.* **1978**, *81* (3), 471–480.
(41) Madelin, T. M.; Johnson, H. E. Fungal and actinomycete spore aerosols measured at different humidities with an aerodynamic particle sizer. *J. Appl. Microbiol.* **1992**, *72* (5), 400–409.
(42) Meadow, J. F.; Altrichter, A. E.; Kembel, S. W.; Kline, J.; Mhuireach, G.; Moriyama, M.; Northcutt, D.; O'Connor, T. K.; Womack, A. M.; Brown, G. Z.; et al. Indoor airborne bacterial communities are influenced by ventilation, occupancy, and outdoor air source. *Indoor Air* **2014**, *24* (1), 41–48.
(43) Méheust, D.; Le Cann, P.; Reboux, G.; Millon, L.; Gangneux, J.-P.; Tischer, C.; Gehring, U.; Chen, C. M.; Kerkhof, M.; Koppelman, G.; et al. Indoor fungal contamination: Health risks and measurement methods in hospitals, homes and workplaces. *J. Allergy Clin. Immunol.* **2014**, *27* (3), 248–260.
(44) O'Meara, T.; Tovey, E. Monitoring Personal Allergen Exposure. *Clin. Rev. Allergy Immunol.* **2000**, *18*.
(45) Patrick, S. K.; Noah, J. A.; Yang, J. F. Developmental constraints of quadrupedal coordination across crawling styles in human infants. *J. Neurophysiol.* **2012**, *107* (11), 3050–3061.
(46) Pereira, M. L.; Knibbs, L. D.; He, C.; Grzybowski, P.; Johnson, G. R.; Huffman, J. A.; Bell, S. C.; Wainwright, C. E.; Matte, D. L.; Dominski, F. H.; et al. Sources and dynamics of fluorescent particles in hospitals. *Indoor Air* **2017**, *27* (5), 988–1000.
(47) Peters, M.; Kauth, M.; Scherner, O.; Gehlhar, K.; Steffen, I.; Wentker, P.; von Mutius, E.; Holst, O.; Bufe, A. Arabinogalactan isolated from cowshed dust extract protects mice from allergic airway inflammation and sensitization. *J. Allergy Clin. Immunol.* **2010**, *126* (3), 648–656.
(48) Pich, J. Theory of gravitational deposition of particles from laminar flows in channels. *J. Aerosol Sci.* **1972**, *3* (5), 351–361.

(49) Pöhlker, C.; Huffman, J. A.; Pöschl, U. Autofluorescence of atmospheric bioaerosols - Fluorescent biomolecules and potential interferences. *Atmos. Meas. Tech.* **2012**, *5* (1), 37–71.
(50) Pringle, A. Asthma and the Diversity of Fungal Spores in Air. *PLoS Pathog.* **2013**, *9* (6), 1–4.
(51) Qian, J.; Ferro, A. R. Resuspension of dust particles in a chamber and associated environmental factors. *Aerosol Sci. Technol.* **2008**, *42* (7), 566–578.
(52) Qian, J.; Hospodsky, D.; Yamamoto, N.; Nazaroff, W. W.; Peccia, J. Size-resolved emission rates of airborne bacteria and fungi in an occupied classroom. *Indoor Air* **2012**, *22* (4), 339–351.
(53) Qian, J.; Peccia, J.; Ferro, A. R. Walking-induced particle resuspension in indoor environments. *Atmos. Environ.* **2014**, *89*, 464–481.
(54) Reponen, T.; Willeke, K.; Ulevicius, V.; Reponen, A.; Grinshpun, S. A. Effect of relative humidity on the aerodynamic diameter and respiratory deposition of fungal spores. *Atmos. Environ.* **1996**, *30* (23), 3967–3974.
(55) Reponen, T.; Grinshpun, S. a; Conwell, K. L.; Wiest, J.; Anderson, M. Aerodynamic versus physical size of spores: Measurement and implication for respiratory deposition. *Grana* **2001**, *40* (3), 119–125.
(56) Reponen, T.; Lockey, J.; Bernstein, D. I.; Vesper, S. J.; Levin, L.; Khurana Hershey, G. K.; Zheng, S.; Ryan, P.; Grinshpun, S. A.; Villareal, M.; et al. Infant origins of childhood asthma associated with specific molds. *J. Allergy Clin. Immunol.* **2012**, *130* (3), 639–644.e5.
(57) Rintala, H.; Pitkäranta, M.; Täubel, M. *Microbial communities associated with house dust*; 2012; Vol. 78.
(58) Robinson, N. H.; Allan, J. D.; Huffman, J. A.; Kaye, P. H.; Foot, V. E.; and Gallagher, M. Cluster analysis of WIBS single-particle bioaerosol data. *Atmos. Meas. Tech.* **2013.** *6* (2), 337–347.
(59) Saari, S. E.; Reponen, T.; Keskinen, J. Performance of Two Fluorescence-Based Real-Time Bioaerosol Detectors: BioScout vs. UVAPS. *Aerosol Sci. Technol.* **2014**, *48* (4), 371–378.
(60) Saari, S. E.; Mensah-Attipoe, J.; Reponen, T.; Veijalainen, A. M.; Salmela, A.; Pasanen, P.; Keskinen, J. Effects of fungal species, cultivation time, growth substrate, and air exposure velocity on the fluorescence properties of airborne fungal spores. *Indoor Air* **2015**, *25* (6), 653–661.
(61) Saari, S. E.; Niemi, J.; Rönkkö1, T.; Kuuluvainen, H.; Järvinen, A.; Pirjola, L.; Aurela, M.; Hillamo, R.; Keskinen1, J. Seasonal and Diurnal Variations of Fluorescent Bioaerosol Concentration and Size Distribution in the Urban Environment. *Aerosol Air Qual. Res.* **2015**, 572–581.
(62) Sagona, J. A.; Shalat, S. L.; Wang, Z.; Ramagopal, M.; Black, K.; Hernandez, M.; Mainelis, G. Evaluation of particle resuspension in young children's breathing zone using stationary and robotic (PIPER) aerosol samplers. *J. Aerosol Sci.* **2015**, *85*, 30–41.
(63) Savage, N.; Krentz, C.; Könemann, T.; Han, T. T.; Mainelis, G.; Pöhlker, C.; and Huffman, J. A. Systematic characterization and fluorescence threshold strategies for the wideband integrated. *Atmos. Meas. Tech. Discuss.* **2017**, https://doi.org/10.5194/amt-2017-170.
(64) Schmidt, C. Pollen Overload: Seasonal allergies in a changing climate. *Environ. Heal. Perspect.* **2016**, *124* (4), 70–75.
(65) Seinfeld, J. H.; Pandis, S. N. *Atmospheric Chemistry and Physics: From Air Pollution to Climate Change*; 2006.
(66) Shalat, S. L.; Stambler, A. A.; Wang, Z.; Mainelis, G.; Emoekpere, O. H.; Hernandez, M.; Lioy, P. J.; Black, K. Development and in-home testing of the pretoddler inhalable particulate environmental robotic (PIPER Mk IV) sampler. *Environ. Sci. Technol.* **2011**, *45* (7), 2945–2950.
(67) Sporik, R.; Holgate, S. T.; Platts-Mills, T. A. E.; Cogswell, J. J. Exposure to house-dust mite allergen (Der p 1) and the development of asthma in childhood. *N. Engl. J. Med.* **1990**, *323*, 502–507.
(68) Stein, M. M.; Hrusch, C. L.; Gozdz, J.; Igartua, C.; Pivniouk, V.; Murray, S. E.; Ledford, J. G.; Marques dos Santos, M.; Anderson, R. L.; Metwali, N. Innate immunity and asthma risk in Amish and Hutterite farm children. *N. Engl. J. Med.* **2016**, *375* (5), 411–421.
(69) Sturm, R. Bioaerosols in the lungs of subjects with different ages-part 1: deposition modeling. *Ann. Transl. Med.* **2016**, *4* (11).
(70) Täubel, M.; Rintala, H.; Pitkäranta, M.; Paulin, L.; Laitinen, S.; Pekkanen, J.; Hyvärinen, A.; Nevalainen, A. The occupant as a source of house dust bacteria. *J. Allergy Clin. Immunol.* **2009**, *124* (4).
(71) Taylor, P. E.; Jacobson, K. W.; House, J. M.; Glovsky, M. M. Links between pollen, atopy and the asthma epidemic. *Int. Arch. Allergy Immunol.* **2007**, *144* (2), 162–170.
(72) Thatcher, T. L.; Lai, A. C. K.; Moreno-Jackson, R.; Sextro, R. G.; Nazaroff, W. W. Effects of room furnishings and air speed on particle deposition rates indoors. *Atmos. Environ.* **2002**, *36* (11), 1811–1819.
(73) Thorne, P. S.; Kulhánková, K.; Yin, M.; Cohn, R.; Arbes Jr, S. J.; Zeldin, D. C. Endotoxin exposure is a risk factor for asthma: the national survey of endotoxin in United States housing. *Am. J. Respir. Crit. Care Med.* **2005**, *172* (11), 1371–1377.
(74) Tian, Y.; Sul, K.; Qian, J.; Mondal, S.; Ferro, A. R. A comparative study of walking-induced dust resuspension using a consistent test mechanism. *Indoor Air* **2014**, *24* (6), 592–603.

(75) Tian, Y.; Licina, D.; Savage, N.; Huffman, J. A.; W.W., N. Size-resolved total particle and fluorescent biological aerosol particle emissions from clothing. *In Proceedings of Indoor Air 2016*; Ghent, Belgium, 2016.
(76) Tischer, C.; Weikl, F.; Probst, A. J.; Standl, M.; Heinrich, J.; Pritsch, K. Urban Dust Microbiome: Impact on Later Atopy and Wheezing. *Environ. Health Perspect.* **2016**, *124* (12), 1919.
(77) Torrent, M.; Sunyer, J.; Muñoz, L.; Cullinan, P.; Iturriaga, M. V.; Figueroa, C.; Vall, O.; Taylor, A. N.; Anto, J. M. Early-life domestic aeroallergen exposure and IgE sensitization at age 4 years. *J. Allergy Clin. Immunol.* **2006**, *118* (3), 742–748.
(78) Tovey, E. R.; Almqvist, C.; Li, Q.; Crisafulli, D.; Marks, G. B. Nonlinear relationship of mite allergen exposure to mite sensitization and asthma in a birth cohort. *J. Allergy Clin. Immunol.* **2008**, *122* (1), 114–118.
(79) U. S. EPA. Exposure factors handbook 2011 edition (Final). Washington, DC, **2011**.
(80) Valkonen, M.; Wouters, I. M.; Täubel, M.; Rintala, H.; Lenters, V.; Vasara, R.; Genuneit, J.; Braun-Fahrländer, C.; Piarroux, R.; Von Mutius, E.; et al. Bacterial exposures and associations with atopy and asthma in children. *PLoS One* **2015**, *10* (6), 1–14.
(81) Velazco-Roa, M. A.; Dzhongova, E.; Thennadil, S. N. Complex refractive index of nonspherical particles in the visible near infrared region--application to Bacillus subtilis spores. *Appl. Opt.* **2008**, *47* (33), 6183–6189.
(82) Von Mutius, E.; Vercelli, D. Farm living: effects on childhood asthma and allergy. *Nat. Rev. Immunol.* **2010**, *10* (12), 861–868.
(83) Wang, Z.; Shalat, S. L.; Black, K.; Lioy, P. J.; Stambler, A. A.; Emoekpere, O. H.; Hernandez, M.; Han, T.; Ramagopal, M.; Mainelis, G. Use of a robotic sampling platform to assess young children's exposure to indoor bioaerosols. *Indoor Air* **2012**, *22* (2), 159–169.
(84) Yamamoto, N.; Hospodsky, D.; Dannemiller, K. C.; Nazaroff, W. W.; Peccia, J. Indoor emissions as a primary source of airborne allergenic fungal particles in classrooms. *Environ. Sci. Technol.* **2015**, *49* (8), 5098–5106.
(85) You, R.; Cui, W.; Chen, C.; Zhao, B. Measuring the short-term emission rates of particles in the "personal cloud" with different clothes and activity intensities in a sealed chamber. *Aerosol Air Qual. Res.* **2013**, *13* (3), 911–921.
(86) Zhang, X.; Ahmadi, G.; Qian, J.; Ferro, A. R. Particle Detachment, Resuspension and Transport Due to Human Walking in Indoor Environments. *J. Adhes. Sci. Technol.* **2008**, *22* (5–6), 591–621.
(87) Zhou, J.; Fang, W.; Cao, Q.; Yang, L.; Chang, V. W.-C.; Nazaroff, W. W. Influence of moisturizer and relative humidity on human emissions of fluorescent biological aerosol particles. *Indoor Air* **2016**, *27* (3), 587–598.
(88) Droplet Measurement Technologies, Inc. *Wideband Integrated Bioaerosol Sensor (WIBS-NEO) Operator Manual*. Boulder, CO, **2016.**
(89) Leaver, I. H.; Milligan, B. Fluorescent whitening agents—a survey (1974-82). *Dye. Pigment.* **1984**, *5* (2), 109–144.
(90) Burg, A. W.; Rohovsky, M. W.; Kensler, C. J.; Wogan, G. N. Current status of human safety and environmental aspects of fluorescent whitening agents used in detergents in the United States. *Crit. Rev. Environ. Sci. Technol.* **1977**, *7* (1), 91–120.